

# Design, Control, and Clinical Applications of Magnetic Actuation Systems: Challenges and Opportunities

Yingxin Huo, Lidong Yang, Tiantian Xu,\* and Dong Sun

The enhancement of medical services relies significantly on engineering research. Magnetic actuation systems (MASs) are designed to be safe for biomedical applications and offer long-distance and dynamic control capabilities, rendering them highly favorable for clinical applications. The integration of MASs with sophisticated perception and positioning methods enhances their suitability for clinical applications. Achieving this goal hinges on the development of MASs and their control methods; thus, a comprehensive review of current technical and scientific issues is indispensable for addressing the related challenges. This review encompasses both the classical and state-of-the-art research, providing readers with a thorough understanding of the intricacies involved in MAS design, system control methods, clinical applications, and guidance toward the next phase of exploration. In addition, a detailed illustration of the underlying principles of the magnetic actuation method is provided, which helps delineate the design principles. A detailed analysis of potential clinical applications in hard-to-reach environments inside the human body provides guidance for interdisciplinary researchers. Challenges and opportunities associated with MAS design and application are summarized to inspire researchers and stimulate innovative explorations. Finally, this review concludes that sustained research in this field has the potential to yield groundbreaking advancements capable of revolutionizing modern medicine.

## 1. Introduction

The commercialization of the da Vinci Surgical System has brought attention to engineering methods used in surgery and demonstrated the potential of robots in clinical use. Researchers have focused on remote actuation methods to achieve the wireless control of untethered robots. The proposed solutions include optical,<sup>[1,2]</sup> acoustically controlled,<sup>[3,4]</sup> chemical reaction,<sup>[5,6]</sup> and magnetic field-based methods.<sup>[7]</sup> Optical tweezers are highly sensitive and flexible tools that trap cells and microparticles. However, their penetration rate through the body is low; thus, the force of the tweezers is too low for their application. An acoustically controlled method can be used as the driving force in the actuation of specially designed microrobots inside the human body without causing harm; however, the direction and trajectory of these robots are difficult to control accurately. Research related to this topic is still in the early stages of development. Chemical reaction methods can actuate a microrobot to move forward; however,

the chemical alterations induced in the body are difficult to control. Compared with the aforementioned methods, the magnetic field method can actuate magnetic robots wirelessly without attenuation during penetration through the human body. Magnetically controlled microrobots can be accurately directed to move inside living bodies to solve numerous medical problems. The disadvantages of magnetic actuation are limited workspace, restricted magnetic flux density for actuation, and the bulk and expense of the designed system. Thus, the development of magnetic actuation systems (MASs) has been aimed at overcoming these limitations.

The interdisciplinary nature of MASs in clinical applications necessitates collaborative efforts from a spectrum of experts, including roboticists, clinical specialists, regenerative medicine scientists, and biomedical engineers. Clinical experts integrate traditional methodologies with engineering analyses to devise solutions to the current challenges.<sup>[8,9]</sup> Researchers in regenerative medicine have concurrently modified stem cells to generate curative effects at specific target sites.<sup>[10]</sup> In terms of biomedical engineering, magnetic micro-/millirobots (MMRs) have been employed as carriers to achieve precise drug delivery utilizing closed-loop control methods.<sup>[11,12]</sup> Specifically, the development of clinically utilized MASs by roboticists and engineers serves as

Y. Huo, D. Sun  
Department of Biomedical Engineering  
City University of Hong Kong  
Hong Kong, China

L. Yang  
The Research Institute for Advanced Manufacturing  
Department of Industrial and Systems Engineering  
The Hong Kong Polytechnic University  
Hong Kong, China

T. Xu  
Guangdong Provincial Key Laboratory of Robotics and Intelligent System,  
and Key Laboratory of Biomedical Imaging Science and System  
Shenzhen Institute of Advanced Technology  
Chinese Academy of Sciences  
Shenzhen 518055, China  
E-mail: tt.xu@siat.ac.cn

 The ORCID identification number(s) for the author(s) of this article can be found under <https://doi.org/10.1002/aisy.202400403>.

© 2024 The Author(s). Advanced Intelligent Systems published by Wiley-VCH GmbH. This is an open access article under the terms of the Creative Commons Attribution License, which permits use, distribution and reproduction in any medium, provided the original work is properly cited.

DOI: 10.1002/aisy.202400403

the foundational element underpinning all these collaborative endeavors.<sup>[13–15]</sup> The synergy of expertise and effort across these disciplines propels the advancement and facilitates innovations that hold significant promise for the future of medical robotics.

The conventional approach to medical treatment often entails the administration of high doses of medication to patients via the bloodstream, relying on passive transportation. However, this method has limitations, as a significant portion of the medication can be absorbed by nontargeted organs or cells, potentially causing side effects and harm to the body. This necessitates a more precise and controlled delivery mechanism. MASs enable the precise untethered control of magnetic robots, allowing for targeted delivery and controlled movement within the body. This capability opens a multitude of clinical applications. Beyond precision drug delivery, MMRs actuated by MASs can facilitate the targeted delivery of functional cells, such as stem cells, to repair damaged cartilage. Moreover, MASs are relevant in various scenarios requiring precise delivery, such as removing blood clots from the cardiovascular system and performing vitreoretinal or gastrointestinal endoscopy. Addressing these diverse applications requires the development of suitable MASs and MMRs that are tailored for clinical use. Significant attention has been devoted to advancing the MAS and MMR designs to satisfy the specific needs of clinical applications, emphasizing their potential to revolutionize the field of medicine.

There are several advantages to using the MAS during surgery. Compared with alternative medical approaches, such as remote-centered robotic-assisted systems utilized in minimally invasive surgery, MAS-controlled mechanisms rely on noncontact forces, making noninvasive surgery possible. The camera is the most frequently used imaging method for providing image feedback in closed-loop control. However, in vivo imaging methods, such as X-ray radiography, computed tomography (CT), and digital subtraction angiography, are most frequently used in modern surgery. Although the magnetic fields employed pose no harm to humans, these imaging methods using ionizing radiation can be harmful if the surgeon is exposed to radiation for long periods. The control of MMRs under MASs has the potential to enable remote surgical interventions. With the ability to perform remote control, a surgeon can be protected from imaging equipment with ionizing radiation. Furthermore, remote surgeries eliminate the constraints related to the operation time and frequency for the surgeon. Due to these advantages, the development of a suitable MAS for clinical applications has attracted attention for several decades.<sup>[16]</sup> Significant advancements have been made in the prototyping and design stages, resulting in various magnetic field generation methods tailored to drive MMRs with specialized locomotion capabilities.

However, designing and implementing actuation systems for clinical applications present inherent challenges. One such challenge arises from the fundamental characteristics of MASs. Specifically, the inherent instability of the dipole in all directions, viewed from an energy standpoint, poses a significant hurdle for effectively controlling permanent MASs. In addition, the drop-off of the magnetic field follows a cubic distance decay from the generation point, which is exceptionally high and often unsuitable for certain applications due to this rapid reduction. Even in scenarios where the magnetic field is intensified at the center of the workspace, the effective workspace is not the entire 3D environment

because of the high gradient near the electromagnet, further complicating the MAS design for practical applications.

To address these challenges and improve the performance of MASs, the closed-loop flux path method has been used to enhance the magnetic field and gradient. This system can be used as a magnetic catheter guidance system with an appropriate mapping method.<sup>[17]</sup> An in-depth analysis of the field distribution in the workspace and between these electromagnets can determine the current required to achieve a specific task.<sup>[18]</sup> The applied current must be carefully regulated to prevent excessive heat generation, which can potentially damage the wire. Furthermore, effective workspaces remain constrained for several practical applications. Recent research has explored advancements, such as wire patterns and coil design,<sup>[19]</sup> to further enhance the manipulation performance with the aim of pushing the boundaries of effective magnetic actuation in complex clinical settings.

Effective control of MMRs plays a pivotal role in their operational efficiency, particularly when these robots work together to achieve complex tasks. The morphology of a robot significantly influences its control and functionality. At present, extensive research has been focused on various modes of movement, such as slipping, rolling, walking, and climbing, as these fundamental modes can be combined to effectively accomplish diverse tasks.<sup>[20]</sup> A critical aspect of the design of MMRs is the material composition, which must exhibit magnetizable properties without cytotoxicity. Notably, the development of MMRs using materials that are both biodegradable and magnetizable has been the focal point of recent research.<sup>[21–23]</sup> The objective is to create robots that enable efficient navigation and propulsion by incorporating multiple locomotion abilities. Moreover, after controlled MMRs have been specified, the design of an MAS capable of producing a sufficiently high magnetic field gradient or torque within a substantial workspace is equally critical. This aspect has been extensively explored in the literature, emphasizing the importance of achieving an MAS design appropriate for ensuring the generation of accurate and high-gradient magnetic fields during the navigation of MMRs.<sup>[17,24–27]</sup> These designs lay the foundation for medical treatments using magnetic manipulations.

Beyond the design of MASs and MMRs, the efficacy of the system depends heavily on the feedback obtained through imaging techniques. Photoacoustic imaging, which is emerging as a promising in vivo imaging modality,<sup>[28]</sup> has gained substantial attention as a feedback signal for modern research applications. Depending on the specific application, other imaging techniques such as fluoroscopy or magnetic resonance imaging (MRI) are also suitable, although shortcomings such as a risk to health and the time-consuming nature exist. Other methods for imaging or localizing magnetic robots have also been developed in recent years. However, these methods have certain limitations. The images detected using magnetic particle imaging are vague, and this imaging method cannot be simultaneously used with magnetic actuation.<sup>[29]</sup> The arrays of Hall sensors can effectively determine the orientation and position of the MMR. However, this method heavily relies on highly sensitive sensor arrays and cannot determine the location of a magnetic robot in real time.<sup>[30]</sup> Another study reported that the inductive detection of microrobots can simultaneously achieve sensing and actuation.<sup>[31]</sup> This method can only work within a limited frequency range to effectively detect the responses of microrobots, and

time-consuming calibration is required, which can introduce additional sources of error. Thus, this creative method is only useful under special circumstances. In addition, limitations in working space, magnetic field selection, and additional sensor placement make it difficult to use this method in clinical practice. Magnetomechanical resonators have been used to develop miniature wireless sensors that can provide real-time feedback under various scenarios.<sup>[32]</sup> Although a magnetomechanical resonator sensor can measure as small as  $0.8 \times 1.9$  mm, it is still too large to be loaded for most MMRs' clinical applications, and the requirements during localization are high. Furthermore, external magnetic or electrical signals should be strictly avoided during applications. Vision-based feedback control remains one of the best options for providing a general solution in clinical applications. In addition to the aforementioned shortcomings, one common problem of the aforementioned methods is that they only reveal information about the magnetic object and not the surrounding tissue or vascular environment; therefore, these methods must be combined with other techniques.

Magnetic robot control can be categorized as individual,<sup>[33]</sup> multiple-agent,<sup>[34]</sup> or robotic swarm control.<sup>[35,36]</sup> Using machine learning and optimization techniques further improves system performance.<sup>[37]</sup> These methodologies have demonstrated promising outcomes, particularly in achieving precise drug delivery within complex 3D environments.

This review aims to provide a broad understanding for interdisciplinary researchers in engineering and clinical applications. The aim of developing MASs is to apply them in the clinical setting; therefore, a comparative study is conducted to describe the standard requirements for the design of an electromagnetic actuation system. The actuation principles, development phases, field types, and force/torque actuation methods are investigated to gain a better understanding of the techniques behind the actuation system design. Furthermore, magnetic robots and MASs used in clinical applications are summarized. The dynamic model of the electromagnet as an actuator is analyzed and a simplified block diagram is mathematically represented. The control methods used in clinical applications are classified as preprogrammed control and control with feedback. Examples are provided to illustrate these methods and verify their effectiveness. MASs and their control techniques are the key methods involved in clinical applications, and the basic principles and classifications are important for interdisciplinary readers to identify the key techniques and choose suitable strategies for their research. Hence, this study details the typical clinical applications classified based on the human body system, and the actuation systems and control methods with specific applications are summarized. This research addresses the development of MASs in clinical surgery and their revolutionary effects in multiple clinical applications. Finally, the challenges and opportunities are outlined to stimulate more innovative research.

## 2. Magnetic Actuation Systems

### 2.1. Magnetic Actuation Principle

To analyze the energy field present in an electromagnetic manipulation system, the first step is to use four Maxwell equations that

form the foundation for representing the electric and magnetic fields.

$$\nabla \cdot \mathbf{E} = \frac{\rho}{\epsilon_0} \quad (1)$$

$$\nabla \times \mathbf{E} = -\frac{\partial \mathbf{B}}{\partial t} \quad (2)$$

$$\nabla \cdot \mathbf{B} = 0 \quad (3)$$

$$\nabla \times \mathbf{B} = \mu_0 \mathbf{J} + \mu_0 \epsilon_0 \frac{\partial \mathbf{D}}{\partial t} \quad (4)$$

where  $\mathbf{E}$  denotes the electrical field strength, which is related to the electric displacement vector  $\mathbf{D}$ ,  $\mathbf{E} = \epsilon_0 \mathbf{D}$ ,  $\epsilon_0$  is the permittivity under vacuum;  $\mathbf{B}$  denotes the magnetic flux density, which is related to the magnetic field strength  $\mathbf{H}$  (A/m);  $\mathbf{B} = \mu_0 \mathbf{H}$  and  $\mu_0 = 4\pi \times 10^{-7}$  (H/m) is the magnetic permeability under vacuum. Electric charge density is represented by  $\rho$ .  $\mathbf{J}$  is the current density (which is zero in the working space and nonzero in the magnets). Other formats that represent Maxwell's equations<sup>[38,39]</sup> are derivatives of Equation (1)–(4).

#### 2.1.1. Magnetic Dipole Field and Stable Analysis

The magnetic dipole model is commonly used to represent the magnetic flux density distribution around one end of a permanent magnet.<sup>[40]</sup> The scalar magnetic potential can be expressed using a Taylor series expansion as follows.

$$\Phi(\mathbf{r}) = \frac{1}{4\pi} \sum_{n=0}^{\infty} \frac{1}{\|\mathbf{r}\|^{n+1}} \int_V \rho^n P_n(\mathbf{r} \cdot \boldsymbol{\rho}) (\mathbf{n} \cdot \mathbf{M}) da \quad (5)$$

where  $\rho$  is the distance away from the center of the magnetic volume to the point of integration,  $P_n(\cdot)$  are Legendre polynomials,  $\mathbf{M}$  is the magnetization,  $\mathbf{n}$  is the normal unit vector, and  $\mathbf{r}$  is the vector from the center of the magnetic volume to the point of interest, which is represented as  $\mathbf{r} = {}^i \mathbf{P}_B - {}^i \mathbf{P}_m$ , as shown in the **Figure 1a**. This equation can be further approximated as a multipole expansion when the points of interest are outside the minimum bounding sphere (the smallest sphere that encompasses the magnet during the analysis of the magnetic flux<sup>[41]</sup>).

The magnetic flux density can be represented with an expansion form as

$$\begin{aligned} \mathbf{B}\{\mathbf{r}, \mathbf{m}\} &= \mu \mathbf{H} = -\mu \nabla \Phi \\ &= \left( \frac{\mu}{4\pi \|\mathbf{r}\|^2} \mathbb{P}_2\{\hat{\mathbf{r}}\} + \frac{\mu}{4\pi \|\mathbf{r}\|^3} \mathbb{P}_3\{\hat{\mathbf{r}}\} + \frac{\mu}{4\pi \|\mathbf{r}\|^4} \mathbb{P}_4\{\hat{\mathbf{r}}\} \right. \\ &\quad \left. + \frac{\mu}{4\pi \|\mathbf{r}\|^5} \mathbb{P}_5\{\hat{\mathbf{r}}\} + \dots \right) \mathbf{m} \end{aligned} \quad (6)$$

where  $\mu$  is the permeability of the surrounding medium; for the free space,  $\mu = \mu_0 \equiv 4\pi \times 10^{-7} \text{ T} \cdot \text{m} \cdot \text{A}^{-1}$ . Notably, permeability is dependent on the distinct medium that holds the MMR.  $\mathbf{m}$  is dipole moment of the object defined by  $\mathbf{m} \equiv \int_V \mathbf{M} dV$ , which is the magnetization  $\mathbf{M}$  on the surface area  $V$ .

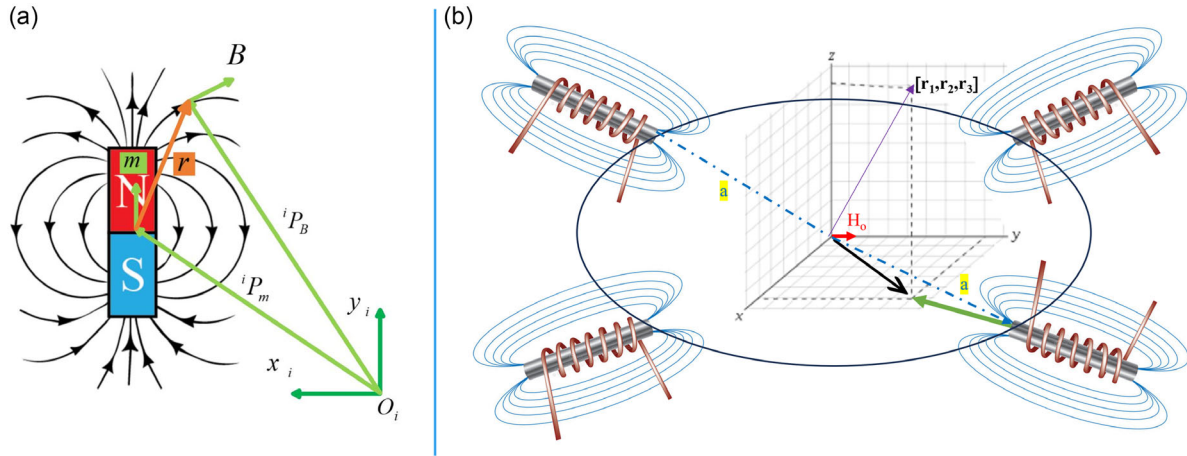


**Figure 1.** Magnetic field illustration. a) The representation of magnetic flux density around a permanent magnet (represented as a magnetic dipole), where the original coordinate is  $x_i - O_i - y_i$ ,  $\mathbf{m}$  represents the magnetic moment,  $\mathbf{B}$  is the magnetic flux density at the position away from the center of the magnetic dipole with a distance  $r$ . b) The multiple electromagnets' field distribution, where the  $[r_1, r_2, r_3]$  represents the position under global coordinate,  $\mathbf{H}_0$  is the unit magnetic field strength, and  $a$  is the radius of the workspace.

Based on the characteristic shown in Equation (3), the even terms ( $\propto \frac{1}{r^2}, \propto \frac{1}{r^4}$ , etc.) are 0 in the expanded form of Equation (6). Therefore, the first nonzero term in the multinomial expansion is the magnitude decays with  $\|r\|^{-3}$  (the dipole term ( $n = 2$ )), the second term decays with  $\|r\|^{-5}$ , and etc.

Based on the advantage that this equation can be used under the condition of an unknown geometry and distribution of a magnet, a simplified approximation is the most frequently used as a reference to estimate the value of the magnetic flux density.<sup>[42]</sup>

$$\mathbf{B}_{\text{dipole}}(\mathbf{r}) = \frac{\mu_0}{4\pi} \frac{1}{\|r\|^3} (3\hat{r}\hat{r}^T - \mathbb{I})\mathbf{m} \quad (7)$$

where  $\hat{r}$  is the unit vector of  $\mathbf{r}$ .  $\mathbb{I} \in \mathbb{R}^{3 \times 3}$  is a unit matrix. According to Equation (7), the strength of the dipole field decays cubically with distance. For the permanent magnets' geometry design, the optimization research of designing the static MAS illustrates that the best shape is in cylinders with a rectangular cross-section (the diameter-to-length ratio is  $\sqrt{4/3}$ ) and a cube, respectively.<sup>[41]</sup>

From an energy standpoint, the total energy  $U_b$  of a magnetic dipole with a moment  $\mathbf{m}$  can be represented as follows.

$$U_b = -\mathbf{m} \cdot \mathbf{B} = -[m_x \quad m_y \quad m_z] \cdot \begin{bmatrix} B_x \\ B_y \\ B_z \end{bmatrix} \quad (8)$$

Earnshaw's theorem provides a fundamental principle that underlies the unstable behavior of a magnetic dipole in an external magnetic field  $\mathbf{B}$ . To ensure that there is a minimum point for Equation (8) to make the magnetic dipole stably levitated, the Laplace equation of  $U_b$  should be greater than zero, that is,  $\nabla^2 U_b > 0$ .

Because both the divergence and curl of  $\mathbf{B}$  are zero, the Laplace equation of  $\mathbf{B}$  is zero, that is

$$\begin{aligned} \nabla^2 U_b &= -\frac{\partial^2 \mathbf{m} \cdot \mathbf{B}}{\partial x^2} - \frac{\partial^2 \mathbf{m} \cdot \mathbf{B}}{\partial y^2} - \frac{\partial^2 \mathbf{m} \cdot \mathbf{B}}{\partial z^2} \\ &= -m_x \nabla^2 B_x - m_y \nabla^2 B_y - m_z \nabla^2 B_z = 0 \end{aligned} \quad (9)$$

Therefore, the dipole cannot reach the minimum or maximum energy points. The dipole cannot be stable in all directions at any point in free space under magnetic field  $\mathbf{B}$ .

To overcome the lack of stable points, researchers have sought solutions by changing the system setup, such as changing the system's accessories to compensate for the unstable direction in the analysis<sup>[43]</sup> or magnetic traps to trap objects at a specific location on 2D surface.<sup>[44]</sup> However, in such situations, if the holding plate or accessories are removed and the analysis is extended to 3D, the object becomes unstable. A similar solution can also be found in magnetic catheter-based guidance systems, where the mechanical reaction force is balanced with the force generated by the magnetic field gradient to achieve stabilization in the field. However, these methods cannot be used in clinical settings with complicated in vivo environments. The unstable effect is a challenge mentioned in some research.<sup>[45]</sup> Another method to bypass Earnshaw's theorem relies on the magnetic field's dynamic control.<sup>[46,47]</sup> The application of time-varying currents to each electromagnet to create a trapping point has been widely used in modern research to achieve adaptive radiation treatment in cancer therapy and selective embolization.<sup>[48,49]</sup> Most existing methods in clinical applications use open-loop pre-programmed controls, which seldom consider dynamic magnetic fields. Another frequently used solution is to employ perception feedback to enhance the control of magnetic robot accuracy to stabilize the movement under the MAS in 3D space.<sup>[14]</sup> The open-loop and closed-loop control methods are described in detail in the following section.

### 2.1.2. Electromagnetic Field and Force/Torque Analysis

The fundamental principle behind the generation of the electromagnetic field is based on Equation (4), which explains the

generation of the magnetic field when an electric field is applied; the second term on the right-hand side shows the hysteresis phenomenon based on the electric displacement.

The force applied to a magnetic object with magnetic dipole moment  $\mathbf{m}$  in field  $\mathbf{B}$  can be represented by the following equation.

$$\mathbf{F} = (\mathbf{m} \cdot \nabla)\mathbf{B} \quad (10)$$

At room temperature,  $\mathbf{m}$  is linearly related to  $\mathbf{B}$  for a superparamagnetic undersaturated magnetic robot. The moment can be represented by<sup>[50]</sup>

$$\mathbf{m} = V_m \mathbf{M} = V_m \frac{\chi_m}{(1 + \chi_m)\mu_0} \mathbf{B} \quad (11)$$

where  $\chi_m$  is the magnetic susceptibility.

Based on Equation (3) and (4),  $\text{tr}(\nabla\mathbf{B}) = 0$  and  $\nabla\mathbf{B}$  is symmetric. These are fulfilled for a magnetic object inside an electromagnetic actuation system workspace. Therefore, the magnetic force can be represented as

$$\mathbf{F} = \begin{bmatrix} \frac{\partial B_x}{\partial x} & \frac{\partial B_x}{\partial y} & \frac{\partial B_x}{\partial z} \\ \frac{\partial B_x}{\partial y} & \frac{\partial B_y}{\partial y} & \frac{\partial B_y}{\partial z} \\ \frac{\partial B_x}{\partial z} & \frac{\partial B_y}{\partial z} & -\left(\frac{\partial B_x}{\partial x} + \frac{\partial B_y}{\partial y}\right) \end{bmatrix} \mathbf{m} \\ = \begin{bmatrix} m_x & m_y & m_z & 0 & 0 \\ 0 & m_x & 0 & m_y & m_z \\ -m_z & 0 & m_x & -m_z & m_y \end{bmatrix} \begin{bmatrix} \frac{\partial B_x}{\partial x} \\ \frac{\partial B_x}{\partial y} \\ \frac{\partial B_x}{\partial z} \\ \frac{\partial B_y}{\partial y} \\ \frac{\partial B_y}{\partial z} \end{bmatrix} = \mathcal{F}(\mathbf{m})\mathcal{G}(\nabla\mathbf{B}^T) \quad (12)$$

Under a simplified situation in which the coordinates of the magnetic field are aligned with the global coordinate, that is,  $\frac{\partial B_x}{\partial y} = \frac{\partial B_x}{\partial z} = \frac{\partial B_y}{\partial z} \equiv 0$ . The magnetic force can be further simplified as follows.

$$\mathbf{F} = \begin{bmatrix} m_x & m_y & m_z & 0 & 0 \\ 0 & m_x & 0 & m_y & m_z \\ -m_z & 0 & m_x & -m_z & m_y \end{bmatrix} \begin{bmatrix} \frac{\partial B_x}{\partial x} \\ 0 \\ 0 \\ \frac{\partial B_y}{\partial y} \\ 0 \end{bmatrix} \\ = \begin{bmatrix} m_x \frac{\partial B_x}{\partial x} \\ m_y \frac{\partial B_y}{\partial y} \\ -m_z \left(\frac{\partial B_x}{\partial x} + \frac{\partial B_y}{\partial y}\right) \end{bmatrix} \quad (13)$$

The magnetic torque is generated through the rotation of  $\mathbf{m}$  about an axis, and its direction is always orthogonal to both  $\mathbf{m}$  and  $\mathbf{B}$ . For magnetic dipole  $\mathbf{m}$  located at the position away from the direction of  $\mathbf{B}$  by  $\theta_x$  about axis  $x$ , the magnetic torque  $\tau_x$  ( $\mathbf{N} \cdot \mathbf{m}$ ) generated is expressed as follows.

$$\tau_x = \frac{\partial(\mathbf{B} \cdot \mathbf{m})}{\partial \theta_x} = \frac{\partial(\|\mathbf{B}\|\|\mathbf{m}\|\cos(\theta_x))}{\partial \theta_x} = -\|\mathbf{B}\|\|\mathbf{m}\|\sin(\theta_x) \quad (14)$$

The total torque in three dimensions can be represented as

$$\boldsymbol{\tau} = \mathbf{m} \times \mathbf{B} = Sk(\mathbf{m})\mathbf{B} \\ = \begin{bmatrix} 0 & -m_z & m_y \\ m_z & 0 & -m_x \\ -m_y & m_x & 0 \end{bmatrix} \begin{bmatrix} B_x \\ B_y \\ B_z \end{bmatrix} \quad (15)$$

where  $Sk(\mathbf{m})$  represents the skew-symmetric form of vector  $\mathbf{m} \times$ . Unlike the three degree of freedom (DoFs) of magnetic force generated, because the magnetic torque cannot be generated about the axis parallel to the direction of  $\mathbf{m}$ , only two DoFs of torque are controllable.

For an MAS comprising multiple electromagnets, as shown in Figure 1b, a linear mapping of the applied current on the coils represents the electromagnetic flux density. The resultant magnetic field at a specific point  $\mathbf{p}$  within the workspace is the summation of the magnetic flux densities generated by each electromagnet. This superposition principle is valid only under the condition that the magnetization remains unsaturated. The current is denoted as  $\mathbf{I} = [I_1, I_2, \dots, I_i, \dots, I_n]^T$  (in amperes), and the resulting summarized magnetic flux density  $\mathbf{B}$  (in Teslas) is represented as follows.

$$\mathbf{B}(\mathbf{p}) = \sum_{i=1}^n \mathbf{B}_i(\mathbf{p}) = \sum_{i=1}^n \tilde{\mathbf{B}}_i(\mathbf{p})I_i \quad (16)$$

where  $\tilde{\mathbf{B}}_i$  is a unit-current vector expressed in Tesla per Ampere.

The partial derivative of  $\mathbf{B}$  with respect to the  $x$ -coordinate at point  $\mathbf{p}$  in the effective workspace can be represented as follows.

$$\frac{\partial \mathbf{B}(\mathbf{p})}{\partial x} = \left[ \frac{\partial \tilde{\mathbf{B}}_1(\mathbf{p})}{\partial x}, \dots, \frac{\partial \tilde{\mathbf{B}}_n(\mathbf{p})}{\partial x} \right] [I_1, \dots, I_n]^T \\ = \sum_{i=1}^n \frac{\partial \tilde{\mathbf{B}}_i(\mathbf{p})}{\partial x} I_i \quad (17)$$

The first item in  $\mathcal{G}(\nabla\mathbf{B}^T)$  of Equation (12), which is  $\frac{\partial B_x}{\partial x}$ , can be represented as  $\sum_{i=1}^n \frac{\partial(\tilde{B}_x)_i(\mathbf{p})}{\partial x} I_i$ . Similarly, the first item in  $\mathbf{B}$  of Equation (15),  $B_x$ , can be represented as  $\sum_{i=1}^n (\tilde{B}_x)_i(\mathbf{p}) I_i$ , where  $(\tilde{B}_x)_i(\mathbf{p})$  represents the magnetic flux density in the  $x$  direction generated by the  $i_{\text{th}}$  electromagnet at position  $\mathbf{p}$ .

By incorporating Equation (12)–(17), a compact representation that considers a controllable magnetic field and field gradient can be obtained, which is expressed as follows.

$$\begin{aligned} \begin{bmatrix} \tau \\ F \end{bmatrix} &= \begin{bmatrix} Sk(m) & \mathbf{O} \\ \mathbf{O} & \mathcal{F}(m) \end{bmatrix} \begin{bmatrix} \mathbf{B} \\ \mathcal{G}(\nabla \mathbf{B}^T) \end{bmatrix} \\ &= \begin{bmatrix} Sk(m) & \mathbf{O} \\ \mathbf{O} & \mathcal{F}(m) \end{bmatrix} \begin{bmatrix} \mathbf{B}(p) \\ \nabla \mathbf{B}(p)^T \end{bmatrix} I \end{aligned} \quad (18)$$

where  $\mathbf{O}$  is the zero matrix. It can be effectively utilized to analyze the electromagnetic forces and torques generated in all three directions. When the magnetic moment of the magnetic object and the unit magnetic flux density in three directions are known, the resulting force and torque applied to the object can be directly correlated with the applied current.

The applied current is derived from the voltage of the input power supply. The change of current applied in the time domain can be represented as

$$\frac{dI(t)}{dt} = \frac{V_c}{L_a} - \frac{R_a}{L_a} I(t) \quad (19)$$

where  $I(t)$  represents the applied current, and  $\frac{dI(t)}{dt}$  denotes the rate of change of the applied current.  $V_c$  stands for the voltage applied to the coil,  $L_a$  and  $R_a$  correspond to the coil inductance and coil resistance, respectively. When multiple coils are actuated simultaneously, mutual induction can be generated between nearby coils. Mutual induction is small and has always been set to 0 in most applications. A more detailed analysis is presented in Section 3.1, and a visual representation is shown in Figure 1b.

In specific applications, on-site calibration methods have been developed to facilitate the straightforward determination of the magnetic field distribution.<sup>[51]</sup> Analytical approaches based on Maxwell's equations have also been used to illustrate the magnetic scalar potential.<sup>[52]</sup> For example, polynomial regression, which utilizes the Laplace equation to introduce flexible field mapping, has been employed in the calculation. To validate the accuracy of the calculation results, the calculation results were compared with the finite-element method simulation results, which can be used to predict magnetic field distributions in untested fields.

## 2.2. Magnetic Actuation Systems

### 2.2.1. Classical Design and Analysis

As mentioned in the previous section, a classical permanent MAS can be achieved using oppositely positioned permanent magnets<sup>[53]</sup> or with a single magnet to generate a gradient magnetic field distribution or a rotating dipole field distribution.<sup>[54,55]</sup>

In contrast, the design of an electromagnetic actuation system is more complex and can be divided into five classical types, as shown in Figure 2a–e.<sup>[56]</sup> The classical and most frequently used designs are Helmholtz and Maxwell coil (HC and MC)-based designs. In the Helmholtz coil, as shown in Figure 2a, when two circular coils with opposite displacements are applied in the same current direction to the coils, the magnetic field between the two coils should be almost uniformly distributed. The diameter of the coil is  $D$ , and the radius of the coil is  $R$ . The figure for the arrow lines indicates the top view of magnetic

induction. The conceptual design and typical prototype of the 3D Helmholtz are shown in Figure 2f–h.<sup>[57]</sup>

Figure 2b, which is a MC-based design, shows that, when the two circular coils are applied with opposite current directions on the coils, the magnetic flux gradient ( $\nabla \mathbf{B}$ ) is generated toward the center of each coil, as indicated by the yellow arrow. The conceptual design and typical prototype for the MAS with an enhanced closed magnetic circuit by adding the bar magnet between two adjacent magnets is shown in Figure 2g.<sup>[17]</sup> Another type of application combines the advantages of both Helmholtz and the MCs, as shown in Figure 2k,<sup>[58]</sup> enabling more DoF force and torque control. Figure 2m<sup>[59]</sup> shows the design merging of three types of basic coils: Helmholtz, Maxwell, and saddle coils. This type of design can be used for 3D locomotion inside human blood vessels to unclog the thrombus.

Figure 2c–e<sup>[56]</sup> shows the electromagnetic field inspired by the MRI system, which is similar to HC and MCs in terms of the field generation principle but with a saddle-shaped coil to generate a uniform, gradient, or transverse direction field distribution. The typical conceptual design and application are shown in Figure 2j,<sup>[60]</sup> respectively, and the design includes a combination of circular and saddle coils.

A typical characteristic of Golay coils (Figure 2e) is that they can be used under the condition that the magnetic field gradient is required at the end of a cylindrical workspace in the direction perpendicular to the main magnetic field. With this unique characteristic, this type of design has the potential to be used in future applications where an accessible workspace is required in the center between two Golay coils.<sup>[61]</sup>

There are two types of design principles for improving the performance of gradient coils: discrete wire and current density methods. Discrete wire methods include longitudinal direction magnetic gradient generation, such as MCs, and transverse direction magnetic gradient generation between two coils, such as Golay coils. Current density methods focus on the wrapping pattern of coils.<sup>[62]</sup> The most frequently used pattern in modern design is the circular pattern.

In terms of quantitative analysis, the Biot–Savart law serves as the foundation for analyzing the electromagnetic field distribution. The magnetic field  $\mathbf{B}$  generated by the current flowing through a wire can be expressed as

$$\mathbf{B}(r) = \frac{\mu_0}{4\pi} \int_C \frac{I d\mathbf{l} \times \mathbf{r}'}{|\mathbf{r}'|^3} \quad (20)$$

where  $r$  is the position away from the wire in 3D space with applied current  $I$ ,  $l$  is the calculated point on the circle  $C$ , and  $\mathbf{r}' = \mathbf{r} - \mathbf{l}$  is the displacement vector.

Based on the Biot–Savart law, the magnetic field on the axis along the center of the wire loop can be represented as

$$B_x(r) = \frac{\mu_0 N I R^2}{2(R^2 + r^2)^{3/2}} = \xi(r) \frac{\mu_0 I}{2R} \quad (21)$$

where  $\xi(r)$  is a distance-dependent coefficient,  $N$  is the number of wires applied,  $I(A)$  is the current applied, and  $R(m)$  is the radius of the coil.

The typical design of a Helmholtz coil is  $R = D/2$ ,<sup>[63]</sup> as shown in Figure 2a. Calculated using Equation (21), the

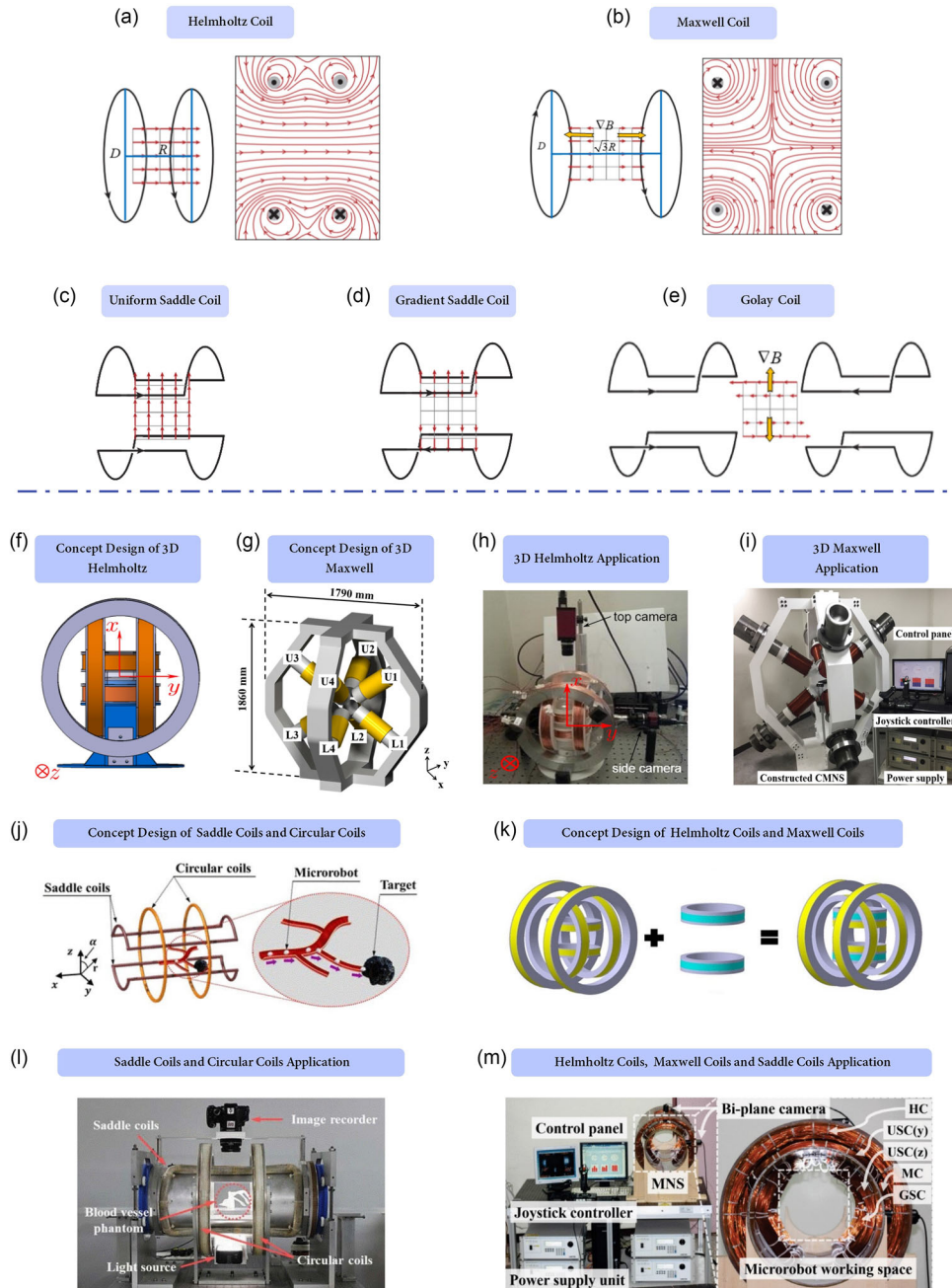


**Figure 2.** Classical design of MASs and their applications. a) Helmholtz coil: two circular coils with diameter  $D$  and distance  $R$  are used to generate a nearly uniform magnetic field when the current flows in the same direction through both coils (adapted from<sup>[56]</sup> with permission). b) MC: two circular coils with diameter  $D$  and distance  $\sqrt{3}R$  are employed to generate a magnetic field gradient ( $\nabla B$ ) when the current flows in the opposite direction through the coils (adapted from<sup>[56]</sup> with permission). c) Uniform saddle coil (USC): two saddle-shaped coils produce a nearly uniform magnetic field when the current flows in the same direction through both coils (adapted from<sup>[56]</sup> with permission). d) Gradient saddle coil (GSCs): two saddle-shaped coils are employed to generate magnetic fields with a gradient directed toward the center of each saddle when the current flows in opposite directions through the coils (adapted from<sup>[56]</sup> with permission). e) Golay coil: this configuration involves two pairs of saddle-shaped coils that generate magnetic fields in the center between them (adapted from<sup>[56]</sup> with permission). f) Conceptual design of three-DoF control with a Helmholtz coil (adapted from<sup>[57]</sup> with permission). g) Conceptual design of three-DoF control with a magnetic field gradient-enhanced Maxwell-inspired coil (adapted from<sup>[17]</sup> with permission). h) Application of a Helmholtz coil with two charge-coupled device cameras installed for three-DoF position control (adapted from<sup>[57]</sup> with permission). i) Application of a magnetic field gradient-enhanced Maxwell-inspired coil with a control panel and power supply for three-DoF position control (adapted from<sup>[17]</sup> with permission). j) Conceptual design of 3D locomotion with a pair of saddle coils and circular coils (adapted from<sup>[60]</sup> with permission). k) Combination conceptual design of the HC and the MC design allows for more DoF control (adapted from<sup>[58]</sup> with permission). l) Experimental implementation of the conceptual design in (j) (adapted from<sup>[60]</sup> with permission). m) Combination implementation of the MC, HCs, GSC, and two USCs [USC(y) and USC(z)] (adapted from<sup>[59]</sup> with permission).

magnetic fields generated at the center point of each coil and in the middle point of the center line are approximately equal, which means the realization of the Helmholtz coil. To realize the MC, the distance between the two coils is set to  $\sqrt{3}R = D$ , and the directions of the current are different. Under this condition, the magnetic flux density at the center is 0, and the second derivative of the field distribution is also 0, indicating that a uniform gradient field is generated. The yellow arrows shown in Figure 2b,e indicate the direction of the magnetic field gradient.

The strength of the magnetic field is directly proportional to the applied current based on Ampere's law. The direction of the magnetic field follows the right-hand rule. For the magnetic field between the two solenoids, the magnetic field  $B$  and moment  $m$  are proportional to the inverse of the square of the distance from the solenoid, that is,  $1/d^2$ , then  $\nabla B \propto 1/d^3$ ,  $F \propto 1/d^5$ ,  $\tau \propto 1/d^4$ .

### 2.2.2. Development Phases and Field Types

Although the application of the MAS can be traced back to the 1920s,<sup>[64,65]</sup> researchers are still trying to solve the issues raised during the application by enhancing the system design. A permanent MAS generates a permanent and uncontrollable magnetic field gradient. However, this characteristic limits its applicability in certain contexts due to the lack of controllability in situations where the positions of the magnets remain static. Subsequently, the orthogonal distributed electromagnetic system was introduced to provide controlled actuation of magnetic objects in orthogonal directions, enabling 3D position control through the utilization of six electromagnets. Despite these advantages, this system is constrained by limitations in the working area, thus making clinical applications difficult.

Recognizing the need for enhanced controllability and expanded working areas, the MAS design has transitioned towards nonorthogonal distributed electromagnets. This design approach has become mainstream in MAS development, overcoming limitations associated with the orthogonal design and facilitating a more versatile and precise magnetic actuation for magnetic robots.

As shown in **Table 1**, the permanent MAS, despite its inherent drawback of a constant and uncontrollable magnetic field gradient, possesses valuable attributes such as an easily adjustable magnitude and cost-effectiveness, rendering it suitable for specific applications, including rotation control,<sup>[66]</sup> the magnetic robot localization within bounded workspaces,<sup>[67]</sup> and particle

sorting.<sup>[68]</sup> However, its limitations, including the constant and uncontrollable magnetic field gradient and restricted control frequency, make it ill-suited for applications demanding precise positioning with rapid on/off switching.

In contrast, the orthogonal electromagnetic system offers a controllable magnetic field gradient in orthogonal directions, facilitating effective decoupled 3D position control. Nevertheless, limitations in its effective workspace and heightened heat generation at high current levels render it unsuitable for applications that require a larger workspace and a higher field gradient or torque.

Compared with the orthogonal electromagnetic system, the nonorthogonal electromagnetic system has a relatively expansive workspace, controllability in multiple directions, and a higher field gradient or torque. It has suitable applications in surgical assistance, MMR delivery, and targeted drug delivery. However, these advantages come at the cost of increased design and control complexity, heightened energy consumption, and the potential for interference with other devices.

Recent research has demonstrated a growing inclination toward combining the merits of robotic arms and magnetic systems in the design of MASs. This hybrid approach has the potential to expand the system's workspace and enhance its flexibility, enabling effective control of MMRs in intricate environments. One notable strategy involves integrating a magnetic tip onto a robotic arm, allowing for the precise positioning and manipulation of MMRs.<sup>[54,69]</sup> Another approach involves leveraging a robotic arm equipped with multiple magnetic coils at its end-point to generate a magnetic field gradient, thereby facilitating the actuation of microrobots or catheters with magnetic end effectors.<sup>[70,71]</sup> These hybrid systems significantly enhance the precision and accuracy of magnetic robot control, rendering them highly suitable for clinical applications. However, it is important to note that these hybrid systems' complexity is higher than the traditional MAS, and they may require advanced control algorithms and application conditions to optimize their performance.

The types of systems were categorized through the papers documented; the data were obtained from Google Scholar and the Web of Science databases from 2005 to 2024. References in relevant publications were further screened. Eventually, 42 high-quality papers and books were used to categorize and demonstrate the evolutionary trends of MAS types.

As shown in **Figure 3** and **Table 2**, the actuation system with the permanent magnet involved is evenly shown from 2005 to

**Table 1.** Advantages and disadvantages of different types of MASs.

Type	Advantages	Disadvantages
Permanent magnetic actuator <sup>[42,66,67]</sup>	Easily adjustable magnitude; energy conservation and low cost; strong and stable magnetic field generation.	Limited DoFs; low frequency in a 3D environment; magnetic field cannot be immediately switched off.
Orthogonal distributed electromagnetic actuator <sup>[14,162]</sup>	Controllable magnetic field; decoupled magnetic force in all dimensions.	Limited effective workspace; power consumption and heat dissipation.
Nonorthogonal distributed electromagnetic actuator <sup>[24,25,38]</sup>	Larger effective workspace; higher magnetic field gradient.	Inflexible and bulky; power consumption and heat dissipation.
Robotic arm with a magnetic end effector <sup>[54,55,81,82,111]</sup>	Extendable workspace; flexible, and easier to install.	Comparatively lower magnetic field gradient.

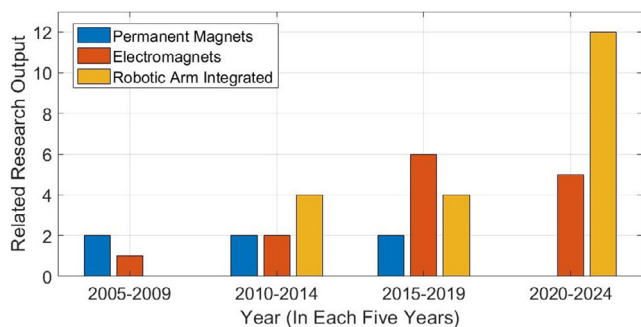


**Figure 3.** MAS development trend.

**Table 2.** Selected papers for categorization.

	Permanent magnets	Electromagnets	Robotic arm integrated
2005–2009	[66,72]	[84]	NA
2010–2014	[68,163]	[38,40]	[54,80,164,165]
2015–2019	[42,67]	[24-26,43,51,85]	[81,82,111,166]
2020–2024	NA	[14,15,161,162,167]	[55,69-71,83,148,168-175]

2019. The orthogonal and nonorthogonal distributed electromagnetic actuation systems were combined and denoted as the electromagnetic actuation system, which is mainly shown from 2015 to 2024. The robotic arm-based actuation systems have been fully developed in recent years, from 2020 to 2024. The trend of MASs use in clinical applications has progressed through several phases with fluctuations and changes from one type to another. The research progressed from the system design to the controller design, then the in vivo applications on animals, and eventually the real-life applications on human beings. Recent research on electromagnetic actuation systems has focused on control theories and applications. Recent research related to robotic arm-integrated systems has focused on reporting the development of the system, the controller design, and the applications within one study.

Throughout the development phases mentioned above, the types of field generation primarily comprise the uniform field, magnetic gradient field, and magnetic torque field. These types of fields are crucial components contributing to the effectiveness and versatility of MASs in various applications, especially in the context of medical interventions. Permanent MASs use a single magnet to generate a stable and constant magnetic gradient.<sup>[67,72]</sup> In addition, an almost uniform magnetic field is generated using two opposing magnets.<sup>[41]</sup> In electromagnetic actuation systems, the magnetic field produced is highly dependent on the current applied to the electrical wires. Adjusting the electrical current enables control over the magnetic field's strength and direction, thereby enabling the generation of multiple magnetic field distributions.

With different current application methods, the electromagnetic actuation system can be artificially separated into two kinds of coils according to the characteristics of the application. Under the condition that torque is the main driving force in the application, typically shown in Helmholtz coils, frequency is a key

parameter. This type of current application method can be called the frequency-based current electromagnetic coil (FCEC). The higher the frequency, the higher the inductive reactance generated in the coil. The rotating magnetic field is a typical example of FCEC applications. Under the condition that the constant current is applied to the coils to generate a magnetic field gradient, it can be called the constant current electromagnetic coil. The inductive reactance is relatively low for this type of application; a typical example is the gradient magnetic field.

Except for the aforementioned, other types of magnetic fields include oscillating magnetic fields, where the strength or direction of magnetic flux density ( $B$ ) changes with time (typically in the shape of a sector or triangle). Oscillating magnetic fields have applications in achieving drug release at the molecular level.<sup>[73]</sup> Moreover, they have been utilized to propel MMRs<sup>[74]</sup> inspired by the motion of bacterial flagella.<sup>[75,76]</sup> The construction of oscillating magnetic fields is relatively straightforward, which includes using the Helmholtz coils or a combination of permanent magnets and a motion control system.<sup>[77]</sup> The oscillating magnetic field driving method is highly related to the morphology and material of the magnetic robot; therefore, it is not a general solution for many clinical situations. Another type of magnetic field that has been applied in medical applications is the pulsed magnetic field.<sup>[78]</sup> This field type is not typically used for driving magnetic robots; hence, this method has always been neglected in MAS research. The typical effective application is using pulsed magnetic fields to stimulate neurons,<sup>[79]</sup> especially in the brain, to treat migraines or depression when standard treatments do not work.

### 2.2.3. Permanent Magnets

**Figure 4** lists the representative permanent magnetic and electromagnetic actuation systems with a timeline sequence. Based on the end effector, the robotic arm-integrated system is listed and separated into permanent and electromagnetic actuation systems. **Figure 4** shows a summary of the design trends. The system design tends to control more DoFs, higher torque, higher gradient, larger workspace, and enhance robotic assistance and collaboration. This trend also represents the development based on the requirements of clinical applications.

Permanent magnets are widely used in the tips of robotic catheters; however, the magnetic force generated between the two permanent magnets cannot be controlled, making the actuation of the catheter difficult when the position is fixed. Early research on permanent magnets aimed to overcome the inherent limitations of being unable to switch the magnetic field on/off immediately and the inability to change the magnetic force, resulting in the proposal of solutions such as adding accessories. For example, researchers explored adding shielding components to magnets to modify the flux density<sup>[72]</sup> or manipulating the system using externally driven magnetic tools<sup>[68]</sup>(**Figure 4a,c**). However, the adding accessories method has a major limitation in real-life applications because of the high requirement for the position of accessories, and only one or two DoFs can be controlled. To further enhance the control capabilities, arrays of permanent magnets were designed to achieve 5-DoF control and create the desired magnetic fields or gradients at specific

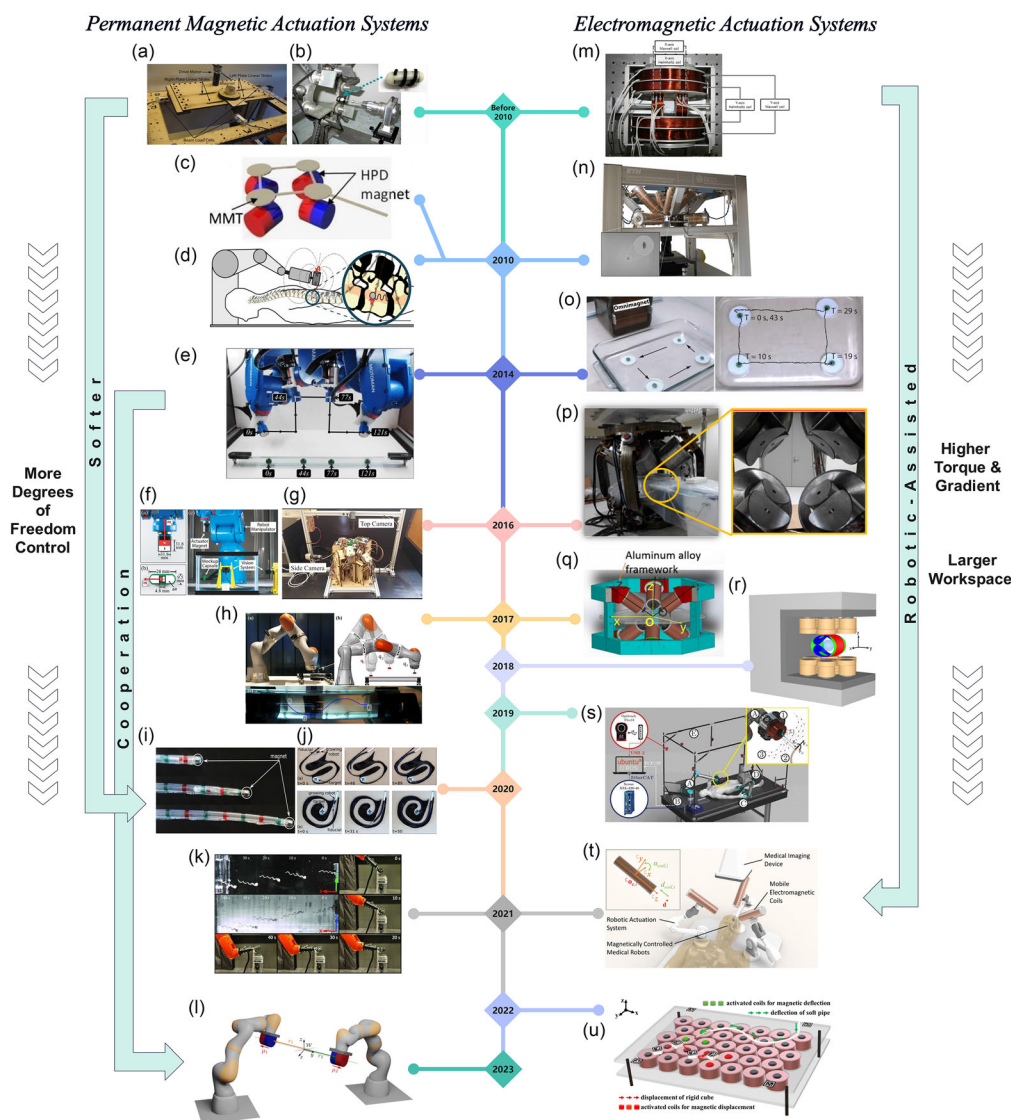


**Figure 4.** Development timeline of representative permanent magnetic and electromagnetic actuation systems. The left part is the development timeline for the permanent magnetic actuators: a) Proof-of-concept design of using shielding materials with permanent magnets to achieve the closed-loop force control (adapted from<sup>[72]</sup> with permission). b) Array of permanent magnets generates the synchronous rotating magnetic field for magnetic robots' driving application (adapted from<sup>[66]</sup> with permission). c) Horizontally two-DoF control method with permanent magnet arrangement and magnetically driven microtools as accessories (adapted from<sup>[68]</sup> with permission). d) One rotating permanent magnet with a robotic arm to remotely control the helical microrobot in 3D space (adapted from<sup>[54]</sup> with permission). e) One permanent magnet combined with the robotic arm generates the rotating and gradient magnetic field to control the magnetic robot in a lumen (adapted from<sup>[80]</sup> with permission). f) Five-DoF magnetic control with one permanent magnet, it can be applied to a stomach capsule endoscope (adapted from<sup>[81]</sup> with permission). g) Five-DoF control with eight rotating permanent magnets, which can reach any magnetic field or field gradient within the limitation (adapted from<sup>[42]</sup> with permission). h) 3D permanent magnet closed-loop position control of microparticles (adapted from<sup>[82]</sup> with permission). i) A ring permanent magnet translucent growing robot (adapted from<sup>[67]</sup> with permission). j) Growing robot, which can be used to achieve curved line movement in vitro (adapted from<sup>[67]</sup> with permission). k) Rotating dipole model-based positioning system in the application of controlling microhelical robots (adapted from<sup>[55]</sup> with permission). l) Two robotic actuated permanent magnets to reach the cooperative remote manipulation (adapted from<sup>[83]</sup> with permission). The right part is the development timeline for the electromagnetic actuators. m) Two pairs of magnetic coil systems (HCs and MCs) to reach the locomotion in 2D (adapted from<sup>[84]</sup> with permission). n) OctoMag: Five-DoF control under the electromagnetic field (adapted from<sup>[38]</sup> with permission). o) Omnimagnet: a single stationary dipole source generates a fully controllable magnetic field and achieves 3D localization (adapted from<sup>[40]</sup> with permission). p) Catheter magnetic navigation system with eight electromagnets to achieve the locomotion inside the heart model (adapted from<sup>[24]</sup> with permission). q) Electromagnet-enhanced actuation system with a large workspace design for minimally invasive therapy (adapted from<sup>[51]</sup> with permission). r) Design of 18 copper coils distributed horizontally with a sufficiently large workspace for clinical applications (adapted from<sup>[85]</sup> with permission). s) Advanced robotics for magnetic manipulation (ARMM) system design to achieve an accurate 3D position control of a microrobot with potential applications in steering magnetic catheters (adapted from<sup>[111]</sup> with permission). t) Conceptual design of RoboMag, in which three robotic arms are combined with three decoupled electromagnetic coils (adapted from<sup>[70]</sup> with permission). u) Planar electromagnetic array actuation system design applied in the deflection of soft pipes and displacement of rigid cubes (adapted from<sup>[161]</sup> with permission).

locations,<sup>[42,66]</sup> as depicted in Figure 4b,g. The fundamental concept behind the design of the permanent magnetic array is to employ rotating magnets and their precise positioning to achieve the intended magnetic flux density and gradient. With this type of permanent magnet-based system, the workspace is larger, and the control dimensions are higher, making it suitable for more clinical situations to control the magnetic catheter inside the natural cavity of humans. As applications have advanced, magnetic actuator designs have gravitated toward more flexible and softer configurations to access deeper regions within the human body. State-of-the-art research has led to the design of a translucent growing robot with the potential for *in vivo* use,<sup>[67]</sup> as illustrated in Figure 4i,j. With the implementation of magneto-inductive sensors, the permanent magnet-based catheters could be localized more accurately.

To further enhance the motion control ability of permanent magnets, most contemporary applications use permanent magnets combined with a robotic arm to accomplish tasks requiring system flexibility, as shown in Figure 4d,e,f,h,k. The earliest research in this area was conducted in 2010,<sup>[54]</sup> as shown in Figure 4d. The purpose of robotic arm integration is to rotate the permanent magnet and scale up the workspace for clinical applications. The innovation of integrating the permanent magnet into the robotic arm coincides with the development of the other two methods, adding accessories and permanent arrays; however, this new method can solve the insufficient workspace problem in application. The earliest systematic analyses of the rotating magnetic fields generated by the permanent magnet at the endpoint of the robotic arm were presented in 2014<sup>[80]</sup> (Figure 4e). The system can be used in any untethered magnetic device control inside the lumen pathways of humans. The aforementioned works used the rotating permanent magnet to achieve the actuation of the helical robot; alternatively, a fixed permanent magnet with robotic arm control could also achieve the positioning of the magnetic robot in 5-DoF; a study published in 2016 reported 3D posing closed-loop control and 2D open-loop orientation control with robotic arm integrated with a permanent magnet,<sup>[81]</sup> as shown in Figure 4f. Another study published in 2017<sup>[82]</sup> (Figure 4h) used the magnetic gradient generated by the permanent magnet for closed-loop position control for accurate drug delivery with the magnetic robot.

Given its ability to achieve accurate position control, this configuration holds significant potential for widespread adoption in multiple clinical applications. Notably, the rotation of the permanent magnet can compensate for the low-frequency nature of permanent magnetic systems. In a study aimed at maintaining the endpoint at a fixed location<sup>[55]</sup> (Figure 4k), the remote control of untethered robots was achieved solely by adjusting the angular velocity of the rotating magnet to modify the required flux distribution. This method ensures a stable and safe distance between the untethered robot and the robotic arm, further enhancing its application potential.

The most recent study has explored the collaboration between two independent serial robotic arms, each equipped with a permanent magnet at the end, to enable magnetomechanical robot control,<sup>[83]</sup> as shown in Figure 4l. This setup allows for the creation of unified and gradient-based magnetic fields within a workspace as expensive as 1000 cm<sup>3</sup>. The effective space for controlling the objects was 50 cm, which represented the

distance between the two permanent magnets. Future research endeavors in this direction should concentrate on expanding the workspace and enhancing the DoFs that the system can control in collaborative robotic systems.

#### 2.2.4. Electromagnets

The development timeline of electromagnetic actuation systems is detailed on the right-hand side of Figure 4. Early designs were heavily influenced by the concepts of HC and MCs.<sup>[40,84]</sup> Figure 4m illustrates a system that combines HC and MCs to achieve 2D preprogrammed position control. However, the application of MAS in clinical requires at least 3-DoF control. The electromagnetic actuation system with multiple electromagnets was designed with a large workspace and unrestrained DoFs<sup>[38]</sup> (Figure 4n). The OctoMag was specifically designed to control intraocular microrobots for retinal surgery. Another method to expand the DoFs in manipulating a magnetic robot is to use a dipole surrounded by electrical wires to achieve control,<sup>[40]</sup> as shown in Figure 4o.

Compared with the traditional design of MASs, the arrangement of multiple electromagnets around a workspace can achieve a larger magnetic field gradient and workspace.<sup>[24,38,51,85]</sup> Figure 4p–r illustrates the various nonorthogonal magnet arrangements. The inclusion of an iron core significantly enhances the magnetic field strength and gradient generated by the electrical coils. In 2015, the study demonstrated that a minimum of eight electromagnets in a symmetrical system could fully control all DoFs,<sup>[86]</sup> leading to the development of eight electromagnets with a back yoke,<sup>[24]</sup> as shown in Figure 4p. This enhanced catheter navigation system with an enlarged workspace and magnetic field gradient can achieve the ablation to treat cardiac arrhythmias. The experiments were conducted in the printed 3D model. Subsequently, a similar design,<sup>[51]</sup> as shown in Figure 4q, was developed to expand the workspace and further enhance the magnetic field gradient. This design can be used in multiple invasive therapies and diagnosis. The development of the system on a clinical scale became the primary focus after the function and control of the system were achieved,<sup>[85]</sup> as shown in Figure 4r, which could be used for cardiac ablation in arrhythmia treatment or steering camera pills for diagnostic video acquisition in the gastrointestinal tract. This system has been proposed for applications in adaptive medical implants, such as adaptive radiation treatment in cancer therapy.<sup>[48]</sup>

**Table 3** summarizes the typical electromagnetic actuation systems designed for clinical applications and their properties. The design criteria included the controllable workspace, maximum magnetic field strength at the center of the workspace under the highest applied current, the highest achievable magnetic field gradient, and the size of the controlled objects. The number of electromagnets was used as a reference to determine whether the system could be fully controlled.

As presented in Table 3, even when all the listed requirements are fulfilled, there are still some limitations in the design of orthogonal and nonorthogonal distributed electromagnet actuation systems, such as inflexibility and bulkiness. To address these issues, approaches that differ in the arrangement of electromagnets, as shown in Figure 4s–u, have been proposed.

**Table 3.** Typical electromagnetic actuation systems and their properties.

	Workspace [mm]	Center $B_{max}$ [mT]	$\nabla B_{max}$ [ $T m^{-1}$ ]	Current [A]	Number of electromagnets	Size of the controlled object
Octomag2010 <sup>[38]</sup>	Hemi-Sphere $\phi 130$	15	0.2	15	8	500 $\mu m$
Diller2016 <sup>[43]</sup>	Cube $120 \times 120 \times 120$	15	0.1	19	8	2 mm
Niu2017 <sup>[51]</sup>	Sphere $\phi 110$	100	2.5	10	6	10 $\mu m$
Rahmer2018 <sup>[85]</sup>	Cylindrical $\phi 200$	400	3	110–140	18	2 cm
Li2019 <sup>[162]</sup>	Circle 2D $\phi 50$	139.2	20.5	10	4	100 $\mu m$
BatMag2019 <sup>[25]</sup>	Sphere $\phi 60 \approx \phi 160$	160	3.575	5	9	350 $\mu m$
ARMM2019 <sup>[111]</sup>	Sphere $\phi 1300$	2350	45	20	1	Magnetically Actuated Catheters
RoboMag2021 <sup>[70]</sup>	Hemi-Sphere $\phi 203$	10	NA (with a 5Hz oscillating field)	5	3	500 nm Microswarm
Array2022 <sup>[161]</sup>	$220.8 \times 162.5 mm^2$	20	1	Unit Current	33	$15 \times 15 \times 8 mm^3$ Cube and a Soft Magnetic Pipe

Figure 4s shows the design of single or multiple robotic arms to achieve a larger workspace for applications in guiding surgical instruments inside the human body. The proposed design can achieve the workspace of the whole human body, which essentially solves the problem of limited workspace.

However, the magnetic flux density and gradient of a single electromagnet are limited. When using a single robotic arm and electromagnet, the magnetic gradient remains relatively uniform within a sphere of radius  $r/2$  at the coil's center. Beyond this point, gradient linearity diminishes rapidly.<sup>[87]</sup> Therefore, multiple electromagnets are incorporated to enhance the magnetic field and gradient, as shown in Figure 4t. A strategy employing three electromagnets on top of three robotic arms arranged around the workspace was proposed to further enhance this setup. The collaborative action of multiple electromagnets further improves the working area and magnetic force; however, it affects the analysis and control of the field distribution with the motion of robotic arms. The application of a robotic arm-based system can be found in the colonoscopy research,<sup>[88]</sup> which was successfully conducted on a pig. The expected time for one colonoscopy was shorter with autonomous magnetic manipulation. The level 3 autonomous inspection enhances the intelligence level in navigation in an unstructured environment, one step closer to application in humans.

Another type inspired by permanent magnetic arrays is to create a 2D infinite space electromagnetic system, as shown in Figure 4u. This approach provides a solution to the limited workspace problem in 2D space. However, extending this type of system to 3D space with the same characteristics remains challenging.

### 2.3. Magnetic Robots

Magnetized robots used in clinical applications primarily comprise tethered catheters or untethered MMRs. The design of the catheter and guidewire often focuses on end-effectors. This study specifically discusses the design of MMRs. Several critical factors must be considered, including the size, locomotion methods, materials, and positioning techniques. **Table 4** lists the relevant parameters and provides representative examples of the designs and applications of untethered robots.

**Table 4.** Important characteristics and representative examples in designing clinically used untethered robots.

Characteristics	Representative examples
Size	30–900 $\mu m$ for microrobots and more than 1 mm for millirobots
Attitude	Drag, roll, twist, walk, and scroll
Number	Single, swarm, and multiagent
Magnetic material	Neodymium magnet (NdFeB), magnetite ( $Fe_3O_4$ ), and strontium hexaferrite ( $SrFe_{12}O_{19}$ )
Nonmagnetic bonding material	$Su_8$ , Hydrogel, and Polydimethylsiloxane
Positioning method	Camera, microscope, ultrasound, optoacoustic imaging, MRI, fluoroscopy, and X-ray radiography

The design of microrobots poses significant challenges to that of millirobots. Their applications primarily target narrow and hard-to-reach environments within the human body. Microrobots are typically defined as robots with a size of less than 900  $\mu m$ . This smaller scale introduces complexities in both the mechanical structure and motion analysis, making the microrobots design more intricate than their millimeter-scale counterparts.

The design of the MMR frequently draws inspiration from nature to satisfy the requirements of locomotion on a small scale. For instance, the MMR designs inspired by fish have evolved from millimeter-scale self-propelling capsule endoscopes driven by alternating magnetic fields<sup>[89]</sup> to microscale fish propelled by oscillating magnetic fields.<sup>[90]</sup> Other bioinspired methods involve nonreciprocal motion to mimic the flexible movement of sperm or the spiral motion of the colon bacillus. Flexible oscillating motion (within an oscillating magnetic field) and helical propulsion (in a rotating magnetic field) have been proposed to facilitate microscale movements. Helical microrobots controlled by rotating magnetic fields are among the most frequently employed setups for microrobot locomotion.<sup>[91,92]</sup> This method is considered to be a superior choice for microrobot locomotion.<sup>[93]</sup>

As research on microrobot design has progressed, various locomotion methods have emerged. Yu et al.<sup>[74]</sup> investigated the motion mechanisms of oscillating magnetically propelled

micro/nanorobots, including wagging, surface walker, and scallop propulsion. Although some designs rely heavily on rotating or oscillating magnetic fields, other devices, such as spherical microrobots<sup>[11]</sup> do not. The typical locomotive attitude of a micro-robot includes dragging, rolling, twisting, walking, or scrolling.

The out-of-equilibrium systems of a swarm have been extensively researched, especially for the collective behavior of multiple microrobots in the microlevel world. Examples include clustering<sup>[94]</sup> (driven by an electric field<sup>[95]</sup> and light<sup>[96]</sup>), flocking,<sup>[97]</sup> or schooling<sup>[98]</sup> and self-organizing behaviors, such as chain,<sup>[99]</sup> ribbon,<sup>[100]</sup> or vortex.<sup>[101]</sup> In summary, propulsion in these systems involves the superposition of magnetic gradient pulling and magnetic torque for rolling or twisting. In such cases, magnetic torque is utilized to generate rotation, which is then converted into propulsion through rolling or twisting. This approach allows for the simultaneous application of magnetic force and torque to achieve propulsion.<sup>[80]</sup> In a swarm of multiple microrobots, the resulting pattern is closely related to the distribution of the magnetic field.<sup>[102]</sup> Specifically, the microswarm pattern is influenced by the ultrahigh aspect ratio of the oscillating magnetic field.

In the field of micro-/nanorobots, the research on multiagent systems is defined as the study of heterogeneous groups of robots, that is, a group of robots with distinct magnetized directions. In such a system, each robot can be individually controlled using a Helmholtz field.<sup>[103]</sup> Because of the heterogeneous nature of MMRs, it is possible to drive different types of MMRs, each with a unique magnetized direction, in different directions and at varying velocities.<sup>[104]</sup> Similar research was also performed in ref. [105].

In terms of manufacturing, 3D microassembly<sup>[106]</sup> is a topic that has been discussed for several years. Designing a microrobot that is biodegradable, magnetizable, and sufficiently small presents manufacturing challenges. In some applications, an excessive size can limit the use of microrobots in *in vitro* experiments, thereby preventing their clinical application. Fortunately, with advancements in microscale manufacturing, microrobots can be produced as small as 30  $\mu\text{m}$ .<sup>[75]</sup> The use of hydrogel has become more prevalent in microrobot designs, making them pliable and softer.<sup>[107]</sup> Magnetic materials are employed to create systems with a strong magnetic response, where nonmagnetic bonding materials are used to render the microrobot softer and biodegradable. Table 4 provides an overview of the typical materials used in microrobot design.

Obtaining visual feedback is critical for determining the position and velocity of a controlled object. The current positioning methods can be categorized into *ex vivo* and *in vivo* methods. *Ex vivo* methods typically involve the use of cameras and microscopes; however, these are unable to penetrate the surface of the human body. By contrast, *in vivo* methods include ultrasonography, optoacoustic imaging, and MRI, which are radiation-free alternatives. However, traditional *in vivo* methods such as C-arm fluoroscopy and X-ray radiography involve radiation. Widespread adoption of non-radioactive methods can greatly enhance surgical procedures. However, some challenges still need to be addressed. Ultrasound images can be unclear, optoacoustic imaging is limited by the penetration depth, and MRI is time-consuming and can conflict with magnetically driven

methods. Therefore, further improvements in this area of research are required.

## 2.4. Applications

Early research on MAS design often centered on evaluating the system performance by analyzing whether the generated magnetic field aligned with expectations based on calibration data or on-site measurements.<sup>[38,68,108–110]</sup> Most studies reported the clinical application as background information and did not present the results of experiments on animals or humans.<sup>[70,111]</sup> Recent high-quality research has begun to investigate practical application challenges and experiments on animals and humans.<sup>[112,113]</sup>

The earliest clinical *in vitro* applications<sup>[114,115]</sup> encompassed the design of the actuation system, modeling, and control, emphasizing the importance of addressing the high gradient generation of an MAS and conducting an analysis of real-life environments. As illustrated in ref. [115], the initial attempt to use MRI for remote control of a ferromagnetic sphere demonstrated its ability to generate a sufficiently large gradient to mimic arterial system navigation. This study also highlighted the need for higher magnetic gradients when using microrobots operated on a smaller scale, such as within capillaries. Since this conclusion, researchers have broadened their focus beyond field generation accuracy to enhance the magnetic field gradient and expand the effective workspace. This shift has addressed the challenges and paved the way for more suitable solutions for clinical applications. The development of a human-scale MAS is expected to remain a primary area of improvement over the coming decades.

Several commercialized products have also been produced in the development history. One of the earliest commercial MASs can be traced decades ago, as mentioned in ref. [116]. This design, known as Niobe and invented by Stereotaxis, Inc. USA,<sup>[117]</sup> utilizes two large permanent magnets. Although bulky, several experiments have demonstrated its applicability in endocardial catheter ablation and gastrointestinal capsule endoscopy. This study also highlighted the challenges of generating a sufficient and stable magnetic field gradient.

Subsequently, the design concept shifted towards nonorthogonal electromagnetic actuation to solve the gradient problem. The catheter guidance control and imaging (CGCI)-Maxwell magnetic navigation system<sup>[118,119]</sup> developed by Magnetecs used eight electromagnets and aims to address the limitations of Niobe and achieve a high magnetic field and rapid response.<sup>[118]</sup> The clinical applications of Niobe include endoscopic capsule procedures<sup>[117]</sup> and percutaneous coronary intervention surgeries.<sup>[120]</sup> However, one limitation of this design is its flexibility. Evolved from CGCI, a new system called Aeon Phocus was designed to enhance installation flexibility and application versatility. This system is divided into two symmetrical parts from the middle to provide an available workspace for the patient. Typical applications include guidance during endoscopy and intravascular surgery.<sup>[121,122]</sup> The most advanced commercial system to date is Genesis (Stereotaxis Inc. USA), which integrates electrophysiological data and a robotic system within the MAS. By 2023, more than 1000 patients with cardiac arrhythmia were treated with this system. The design of a flexible robotic arm and

intelligent sensor integration makes this system a promising solution for modern design.

### 3. System Modeling and Control

#### 3.1. Dynamic Modeling of the Electromagnetic Actuator

In a simplified magnetic robot motion analysis, the quasistatic motion can be analyzed as<sup>[123]</sup>

$$m\dot{\mathbf{v}}(t) = \mathbf{F}_m - c \circ \mathbf{v}(t) + \Delta \quad (22)$$

where  $\mathbf{v}(t)$  is the velocity of a controlled object,  $c$  is the total drag coefficient,  $\circ$  means the element-wise product, and  $\Delta$  is the disturbance. Only  $\mathbf{F}_m$  is controllable; the others change with the surrounding environment and the controlled object.

For the electromagnetic system analysis, the dynamics of the magnetic field strength  $\mathbf{H}(r)$  can be modeled using the applied voltage  $\mathbf{u}(t)$ . According to Equation (6), the magnetic field strength can be transferred to the magnetic flux density with a parameter magnetic permeability  $\mu$ ; therefore, in the following sections,  $\mathbf{H}(r)$  was used in the analysis.

As shown in Figure 1b, to analyze a circularly bounded working area (with radius  $a$  and center at the origin of the global coordinate system) surrounded by  $n$  electromagnets, the total magnetic field strength in position  $r$  at time  $t$  is denoted as  $\mathbf{H}(r, t) = \sum_{k=1}^n \tilde{\mathbf{u}}_k(t) \mathbf{H}_k(r)$ , where  $\mathbf{H}_k(r) \in \mathbb{R}^3$  is the magnetic field strength generated by the unit voltage at position  $\mathbf{r} = [r_1, r_2, r_3]^T$  in 3D space originated from the center of the workspace.

As shown in Figure 1b, only four electromagnets were considered, and a 2D space was used in this analysis.  $\mathbf{H}_o$  is denoted as the magnetic field strength distribution around the lower right corner electromagnets and points in the right direction, and  $\mathbf{H}_k(r)$  can be represented (through a rotation and translation matrix) in global 2D coordinates as

$$\mathbf{H}_k(\mathbf{r}) = -\mathbf{O}_k^T \mathbf{H}_o(a\mathbf{e} - \mathbf{O}_k \mathbf{r}) \quad (23)$$

where  $\mathbf{e} = [1, 0]^T$  for 2D space analysis, and the rotation matrix  $\mathbf{O}_k$  is represented as

$$\mathbf{O}_k = \begin{bmatrix} \cos(2\pi(k-1)/n) & \sin(2\pi(k-1)/n) \\ -\sin(2\pi(k-1)/n) & \cos(2\pi(k-1)/n) \end{bmatrix} \quad (24)$$

The aforementioned is a general method to represent the magnetic field distribution around a circular workspace with four electromagnets around.

High resistance and inductance exist in a high-gradient electromagnetic actuation system. The applied voltage is denoted as the control input  $\mathbf{u}(t) = [u_1(t), u_2(t), \dots, u_n(t)]^T$ , and the required voltage-state vector used to apply the magnetic field strength is represented as  $\gamma_k(t) = R_k I_k(t)$ .

The electromagnetic flux generated by the  $k_{th}$  electromagnet is  $\phi_k = \sum_{j=1}^n L_{kj} I_j$ , then  $\dot{\gamma}_k = u_k - \dot{\phi}_k = u_k - L\dot{I}$ ; therefore, the state space equation is listed as

$$\begin{cases} \dot{\mathbf{I}}(t) = \mathbf{R}^{-1} \boldsymbol{\gamma}(t) \\ \dot{\boldsymbol{\gamma}}(t) = -\mathbf{R}\mathbf{L}^{-1} \boldsymbol{\gamma}(t) + \mathbf{R}\mathbf{L}^{-1} \mathbf{u}(t) \end{cases} \quad (25)$$

$$\mathbf{R} = \text{diag}(R_1, R_2, \dots, R_n); \mathbf{I}(t) = [I_1(t), I_2(t), \dots, I_n(t)]^T \quad (26)$$

where the inductance matrix  $\mathbf{L} \in \mathbb{R}^{n \times n}$  is a symmetric constant matrix, the diagonal elements are  $L_{kk}$  denoted as the inductance of the  $k_{th}$  electromagnet, and  $L_{jk} = L_{kj}$  is denoted as the mutual inductance between two electromagnets  $j$  and  $k$ . State space Equation (25) can also be derived from Equation (19).

The notation in Equation (25) can be simplified by letting  $\xi \mathbf{A} = \mathbf{R}\mathbf{L}^{-1}$ . When  $k$  electromagnets have the same inductance and are symmetrical to each other, all  $L_{kj}$  are equal to zero; therefore,  $\mathbf{A}$  can be the identity matrix, and the state space equation can be represented by only one parameter  $\xi$ .

$$\mathbf{H}(r, t) = \mathbf{H}(r) \boldsymbol{\gamma}(t) \quad (27)$$

$$\mathbf{F}_m(r, t) = K \nabla ||\mathbf{H}(r, t)||^2 \quad (28)$$

$$\mathbf{F}_m(r, t) = 2K \left\{ \frac{\partial [\mathbf{H}(r) \boldsymbol{\gamma}(t)]}{\partial r} \right\}^T \mathbf{H}(r) \boldsymbol{\gamma}(t) = K_f g(\mathbf{r}(t), \boldsymbol{\gamma}(t)) \quad (29)$$

where  $K$  is volume and magnetic permeability-related parameters (refer to Equation (10) and (11)).

$K_f$  contains the parameters  $\xi$ , and  $K$ . The electromagnetic field is only related to the real-time position  $r(t)$  and real-time voltage  $\boldsymbol{\gamma}(t)$ , with a mapping of  $g(\cdot)$ .

According to Equation (22) and (29), the motion analysis is simplified to

$$m\dot{\mathbf{v}}(t) = K_f g(\mathbf{r}(t), \boldsymbol{\gamma}(t)) - c \circ \mathbf{v}(t) + \Delta \quad (30)$$

According to Equation (25), (26), and (30), the complete dynamics of the electromagnetic actuator and the plant are

$$\dot{\boldsymbol{\gamma}}(t) = -\xi \mathbf{A} \boldsymbol{\gamma}(t) + \xi \mathbf{A} \mathbf{u}(t) \quad (31)$$

$$\mathbf{v}(t) = \dot{\mathbf{r}}(t) \quad (32)$$

$$\dot{\mathbf{v}}(t) = \sigma_m K_f g(\mathbf{r}(t), \boldsymbol{\gamma}(t)) - \sigma_m c \circ \mathbf{v}(t) + \sigma_m \Delta \quad (33)$$

where  $\sigma_m = 1/m$ .

#### 3.2. Control

##### 3.2.1. Preprogrammed Control

The pre-programmed control is widely used in several applications<sup>[13,124,125]</sup> where the feedback is not easily acquired in these clinical applications. In this situation, the time-varying position trajectory sequence of the permanent magnet or the sequence of the current input to the electromagnetic system is predefined to control the path of the magnetic object. For electromagnetic actuation systems, the performance of the proposed method is highly dependent on the design of coils, and recent research has begun to consider the optimization of coil design,<sup>[19]</sup> which is also shown as a future trend in MAS design.

The magnetic moment is not easily obtained in real time. The required magnetic field is mapped to the desired moment,

as shown in Equation (11), which is a general solution used for magnetic force control. This mapping is represented by  $m = \mathcal{D}(B)$ .

To symmetrically analyze and control the electromagnetic field and the gradient, according to Equation (16) and (18), the control input and output can be further represented as

$$\underbrace{\begin{bmatrix} B \\ F \end{bmatrix}}_{\text{Output}} = \underbrace{\begin{bmatrix} \mathbb{I} & \mathbf{0} \\ \mathbf{0} & \mathcal{F}(\mathcal{D}(B)) \end{bmatrix}}_{\text{Second}} \underbrace{\begin{bmatrix} B(p) \\ \nabla B(p)^T \end{bmatrix}}_{\text{First}} \underbrace{I}_{\text{Input}} \quad (34)$$

where  $\mathbb{I} \subseteq R^{3 \times 3}$ ,  $\mathcal{D}(B)$  maps the magnetic field applied to the moment of controlled objects.

The physical meaning of Equation (34): the magnetic field and gradient are generated based on the current as the input; then, the controlled object is magnetized with the moment during the interaction with the generated magnetic field.

The preprogrammed control of the MAS can be divided into three types based on the controllable DoFs. The first type is 3-DoF heading or named rotational control. A typical MAS is shown in Figure 2f, where the objects' magnetic moment or torque is controlled, and the magnetic force is neglected. The second type is 3-DoF force control, in which the objects' moments are usually assumed to be aligned with the current magnetic field applied for superparamagnetism or constrained in a predefined direction for magnetized ferromagnets; a typical MAS is shown in Figure 2g. The third type is 5-DoF control, including heading (2-DoF) and force control (3-DoF); a typical MAS is shown in Figure 4n. In special cases that can achieve full 6-DoF control, this type of application concentrates on the creation of torque around the magnetized axis.<sup>[43,110,126]</sup> The trick is to control the magnetic torque, which is nonparallel to the magnetization direction, under the nonuniformity assumption.

The open-loop preprogrammed control method involves programming the required magnetic field, such as a unified, rotating, or oscillating magnetic field, to achieve the required motion or path.<sup>[103]</sup> Furthermore, preprogram control can also be used to control the swarm shape,<sup>[127]</sup> and its application is promising in medical treatment.<sup>[47,49]</sup>

The aforementioned field alignment force and torque control are proposed to control the MMR towards the required

direction.<sup>[40]</sup> The disturbance generated by the attractive force between MMRs or other disturbances can affect motion control; therefore, the following sections focus on the feedback-based control method to enhance the accuracy of preprogrammed control.

### 3.2.2. Control with Feedback

Figure 5 illustrates the overarching control framework governing the MAS. The system comprises three distinct modules: the planning module, the learning module, and the control module. The planning module is the initial stage and is responsible for several tasks. This involves mapping the environment and selecting an appropriate locomotive strategy. Subsequently, this module is engaged in path planning. In some special cases where the trajectory is known, a predefined trajectory sequence is listed to replace path planning.<sup>[128–130]</sup>

The control module assumes the role of devising a controller based on the established model. Most controllers are aimed at position or velocity control. To achieve a controlled position or velocity, the requisite position ( $P_M$ ) for the permanent magnet or the required current ( $I$ ) for the electromagnetic system is output to regulate the MAS. The real-time imaging feedback is usually harnessed to continually minimize the disparity between the real-time position ( $p_r$ ) and the desired position ( $p_d$ ).<sup>[14]</sup> In specific applications, feedback mechanisms such as Hall effect sensors or force sensors play a pivotal role in refining the required magnetic flux density ( $B$ ) or force ( $F$ ) by providing accurate feedback.<sup>[131]</sup> The learning module is integral to estimating unknown parameters encountered during dynamic modeling or controller design. Using this learning module, the system can learn the magnetic actuation principle and adapt to it accordingly.

The entire dynamic system, consisting of the actuator and the plant, represented by Equation (31–33), can be analyzed by dividing the nonlinear system. By separating the linear and nonlinear systems in Equation (33), the nonlinear system can be represented as

$$x(t) = g(r(t), y(t)) \quad (35)$$

where physical meaning of  $x(t)$  is the electromagnetic force.

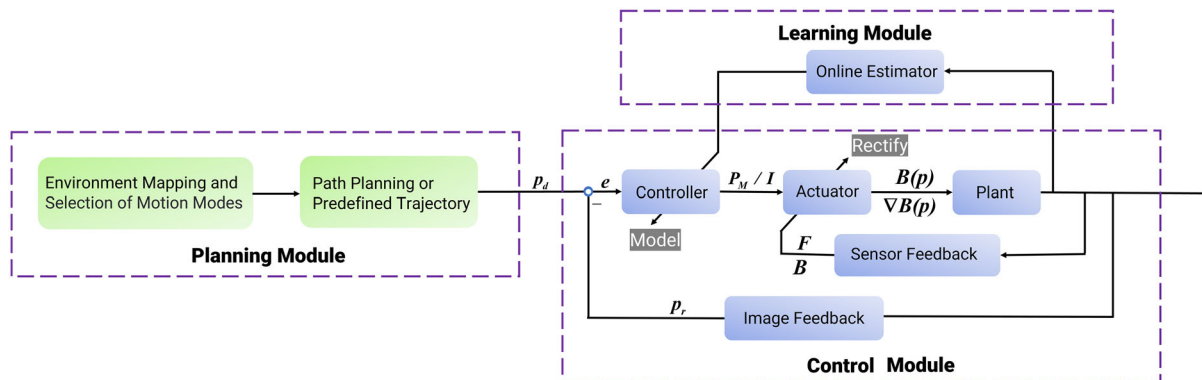


**Figure 5.** General control scheme for MAS-based robot control with sensing feedback and online estimation. Notably,  $p_d$  is the desired position,  $p_r$  is the real-time feedback,  $e$  is the error defined as  $p_d - p_r$ , and  $P_M/I$  is the position of the end effector for the permanent magnet actuator or the current input for the electromagnetic actuator.

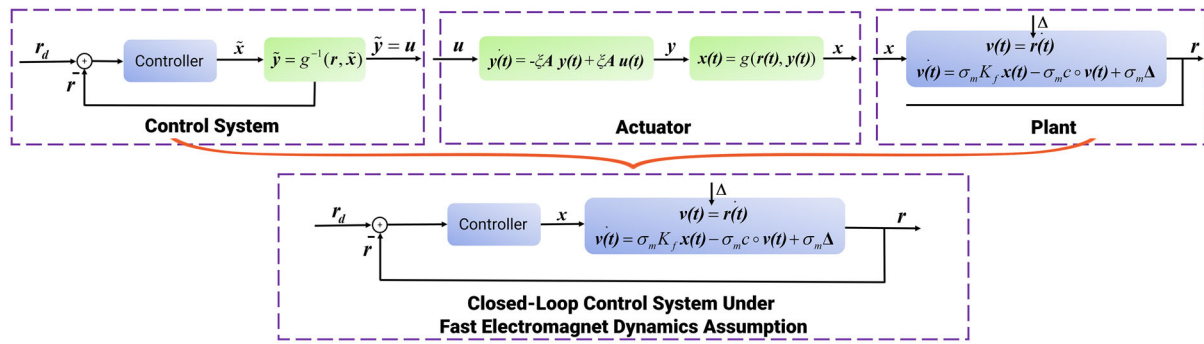


**Figure 6.** The subsystems of the control system, actuation system, and plant; under the fast electromagnetic dynamics assumption, the system can be simplified as the linear controller with the magnetic objects' motion dynamics.

The detailed equations of the block diagram for the controller, actuator, and plant are shown in **Figure 6**. The applied voltage  $u(t)$  is used as the input for the actuation system Equation (31), and the state vector  $x(t)$  is used to represent the electromagnetic force to link the other two subsystems, as represented by Equation (32) and (33).

Representing all vectors with state  $x$ , the nonlinear system in Equation (35) is represented as

$$x = g(r, g^{-1}(r, x)) \quad (36)$$

Under real-life applications, the dynamic system of electromagnetic actuation ensures that the frequency of the subsystem represented by Equation (31) is significantly faster than the closed-loop control system dynamics. Under the condition that  $A$  is an identity matrix, the system can be simplified as the input  $y(t)$  is asymptotically equal to the input  $u(t)$ .

A nonlinear controller was proposed through feedback linearization with Equation (36) as

$$\tilde{y} = g^{-1}(r, \tilde{x}) \quad (37)$$

where  $\tilde{y}$  and  $\tilde{x}$  are the estimation values of  $y$  and  $x$ . The controller design was simplified after cascading the nonlinear controller, as represented by Equation (37). Under the assumption of fast electromagnetic dynamics, the results of the combination are shown at the bottom of **Figure 6**.

Most studies used a simplified system under the fast electromagnetic dynamics assumption to design the controller and achieve position and velocity control. The proposed classical controller includes a linear controller such as proportional integral derivative control, linear-quadratic regulator control, and model predictive control.<sup>[132,133]</sup> In some applications, linear controllers and nonlinear filters are included in the system.<sup>[134]</sup> Classical nonlinear controllers include adaptive control and sliding mode control.<sup>[135]</sup> A typical path planning method<sup>[128,129]</sup> for fulfilling the autonomous control scheme is the rapidly exploring random tree method. In the learning model, iterative learning and deep learning are used to estimate unknown parameters.<sup>[136,137]</sup> A fuzzy logic-based control scheme is induced to manage complex cases.<sup>[138]</sup>

The preprogrammed control and the dynamic control of the magnetic field are widely observed in clinical applications to achieve tasks, such as selective embolization<sup>[49]</sup> or stem cell

delivery inside a high-viscosity joint fluid.<sup>[13]</sup> Position control accuracy is important in precise delivery applications; therefore, feedback control is more widely used in intravascular drug delivery<sup>[113]</sup> or endoscopy.<sup>[88]</sup>

#### 4. Clinical Applications

The utilization of MASs in medical treatment can be traced back to 1985 when an oscillating magnetic field was employed for drug release.<sup>[73]</sup> In contemporary times, research and applications in this domain have significantly progressed. In the following sections, applications at the research or clinical trial stages for hard-to-reach areas inside the human body that hold the potential for future utilization (see **Figure 7**) are investigated. This review is focused on developing new medical treatments for various diseases. The advantages of MASs in surgery are the enhancement of the accuracy level, ease of use even for new clinicians, and reduced pain for the patient through less invasive and time-efficient surgery. Difficulties in the actions of magnetic robots inside the systems shown in **Figure 7** differ based on the characteristics of the disease and the environment in which the surgery is conducted.

Diverse environmental factors underscore the inherent variations in the system analysis of medical treatments across different regions of the human body. For instance, intravascular applications necessitate the consideration of factors such as blood flow speed and vessel size. Environments such as the intraocular, gastrointestinal, and respiratory systems and human joints possess natural cavity passages or accessible surfaces, rendering magnetic robots viable for easy clinical access. Compared with naturally cavitated environments, the essential utility of MASs emerges in medical treatment within unreachable spaces where traditional or continuum robotic-based systems are inadequate. The brain, intravascular system, and urogenital system are notable examples of such environments. **Table 5** presents the representative applications of seven different systems inside the human body, clinical application types, MASs employed, control methods, magnetic robots, imaging techniques, clinical stages reported in the research, and the presence of tethering.

Except for the representative examples, clinical applications in various human systems are explained in terms of the experimental design, control algorithms, and validation process. Control and actuation strategies vary based on the distinct human

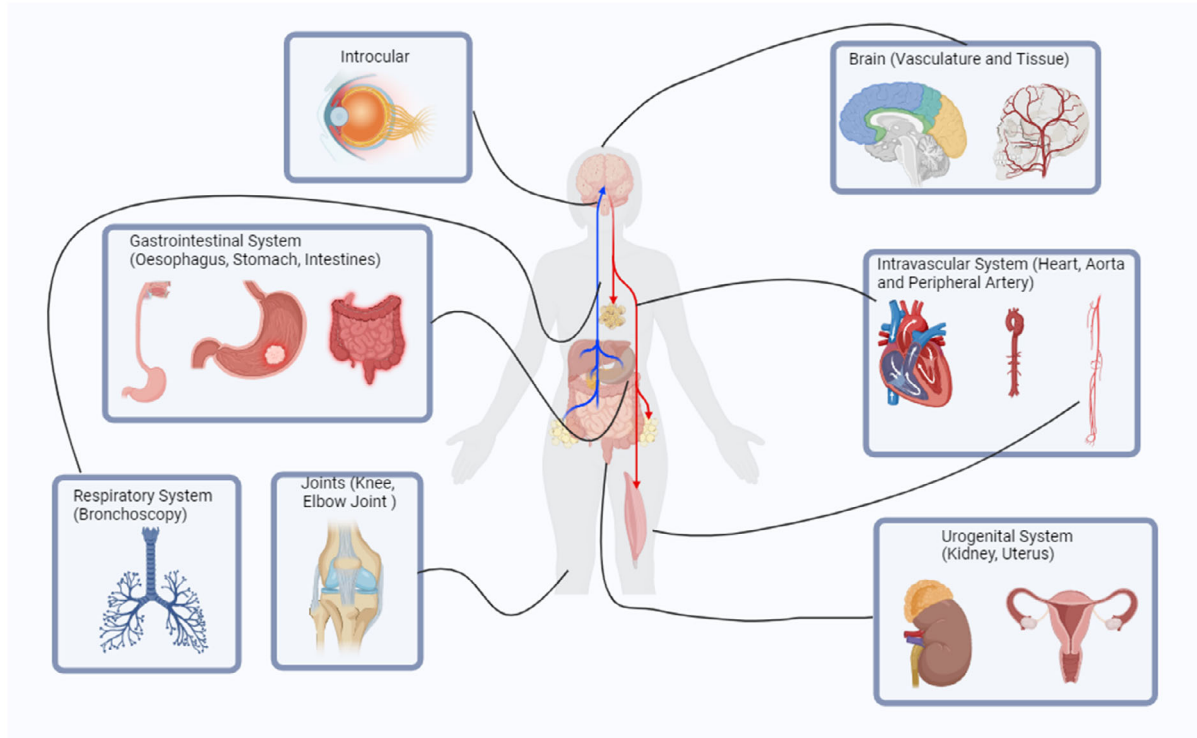


**Figure 7.** Potential environments for using MASs to control magnetic robots in hard-to-reach areas inside the human body.

systems or organs. Considering the distinct challenges in accessing these regions, the implementation of untethered magnetized objects for drug or cell delivery, capsules embedded with magnets for endoscopic applications, and tethered continuum robots equipped with magnetized end-effectors designed for surgical interventions have been explored with detailed clinical examples.

#### 4.1. Brain

The human brain consists of the cerebrum, cerebellum, and stem, collectively classified as brain tissue; the other part is the vascular environment of the brain. The study of the MASs applied to animals (canine brain) can be traced back to 1990<sup>[16]</sup> when a 5 mm-cylindrical permanent magnet was magnetically guided in the intraparenchymal brains of five adult canines to treat brain cancer, such as deliver drugs and take biopsy samples. In this research, traditional electromechanical ball screws were employed to control the motion of the electromagnets. Two canines were scanned with MRI to predefine a coronal reference path. Three canines were used for real-time imaging, and a permanent magnet was stereotactically guided to the predefined position. All five dogs survived the experiments. Although the magnets used in the experiments were too large for human trials, this study demonstrated the feasibility of remotely controlling untethered magnetized robots through a magnetic-driven system for clinical applications, such as the placement of hyperthermic heat lesions or targeted biopsies.

Recent research has utilized permanent magnet arrays to establish a strong magnetic force trap.<sup>[123]</sup> This approach enabled

robots to be attracted to traps without active control. The planar linear stage and one rotational axis were implemented to control the position of the microrobot inside the porcine brain. The magnetic array was responsible for positioning the traps. Ex vivo experiments were conducted on porcine brains using fluoroscopic images to track real-time positions, further underscoring the potential of MMRs for drug delivery, biopsy tasks, hyperthermia, and cauterization. A limitation of this study is its limited workspace of only 6 cm.

In addition to addressing movements within the brain tissue, the control of motion within the brain vasculature represents a crucial research focus. Given the constrained dimensions of the vascular environment, recent cutting-edge research has led to the development of cell-sized microrobots, complemented with real-time optoacoustic tracking to achieve in vivo tracking.<sup>[28]</sup> The 3D real-time tracking of a microrobot in the murine cerebral vascular system has been achieved for the first time. The microrobot was coated with Ni and Au to achieve the imaging and magnetic response simultaneously. Magnetic actuation was achieved using a bar permanent magnet, and the operation was performed manually. This successful experiment laid the foundation for ensuring safe and precise real-time operation within the vascular network of the brain.

#### 4.2. Intravascular System

When deploying microrobots or catheters within human blood vessels, the primary challenge is the varying diameters of the vessels that must be navigated to access the circulatory system. The human body comprises three main types of blood vessels:

**Table 5.** Clinical applications of MASs.

Clinical applications	MASs	Control	Magnetic robot	Imaging	Clinical stage	Untethered
Brain tumor treatment <sup>[16]</sup>	Electromagnets and ball-screw	Ball-screw table control	Permanent magnet (5 mm)	Fluoroscopy and MRI	Canine brain	Y
Brain tissue surgery <sup>[123]</sup>	Permanent magnet array	Magnetic array trapping and motors	NdFeB with polymer housing	Fluoroscopic X-ray	Porcine brain	Y
Brain vascular surgery <sup>[28]</sup>	Permanent bar magnet	Manually	Microrobots	Optoacoustic tomography	Mouse brain	Y
Endocardial catheter ablation <sup>[117,139]</sup>	Stereotaxis Niobe	Preprogrammed magnetic direction control	Magnetic catheter	Fluoroscopy	Human	N
Peripheral arterial disease surgery <sup>[131]</sup>	Helmholtz coils	Magnetic sensor-based Preprogrammed control	Magnetic catheter	Digital microscope video	Vascular phantom	N
Aneurysm embolization <sup>[124]</sup>	Robotic-assisted permanent MAS	Preprogrammed control	Self-adhesive microgels swarm	Fluoroscopy and US	Ex vivo human placenta	Y
Intravascular surgery <sup>[125]</sup>	Helmholtz coils	Preprogrammed control	Claw-engaged microrobots	OCT catheter	Rabbit jugular vein	Y
Improved endovascular access <sup>[113]</sup>	Navion system	Control with visual feedback	Helical magnetic continuum robot with articulated magnetic tip	X-ray	Ex vivo human placenta and a live pig	N
Intraocular surgery <sup>[146]</sup>	Octomag	Preprogrammed motion control	Cylindrical microrobots	Microscope	Rabbit eye	Y
Intraocular surgery <sup>[46]</sup>	Electromagnetic actuation system	Preprogrammed control	Microrobot swarm	Camera/OCT	Bovine eye	Y
Knee cartilage regeneration <sup>[13]</sup>	Electromagnetic actuation system	Precalibrated control	Medical microrobots	Optical microscope or arthroscope	Rabbit knee	Y
Gastrointestinal capsule endoscopy <sup>[117]</sup>	Stereotaxis Niobe	Preprogrammed Control	Video capsule	Fluoroscopy	Human	Y
Stomach capsule endoscopy <sup>[80,81]</sup>	Robotic-assisted permanent MAS	Robotic arm control	Mockup capsule	Camera	Fluid-distended stomach	Y
Autonomous colonoscopy <sup>[88]</sup>	KUKA with a permanent magnet	Autonomous control	Magnetic flexible endoscope	Camera	Female pigs	N
Stomach incisions treatment <sup>[149]</sup>	Helmholtz coils	Preprogrammed control	Microwalker	Camera	Cell slice surface	Y
Stomach ulcers treatment <sup>[151]</sup>	Electromagnetic actuation system	Preprogrammed dynamic control	Soft film-like layers	Ultrasound imaging	Porcine stomach	Y
Lung inspection <sup>[152]</sup>	8-coil MAS	Estimation-based catheter control	Magnetic endoscope	Camera	Lung phantom	N
Autonomous bronchoscopy <sup>[153]</sup>	Dual-arm MAS	Precomputed robotic control	Optimized magnetic catheter	Visual analysis	Bronchial phantom	N
Retrograde intrarenal surgery <sup>[154]</sup>	5-coil orthogonal MAS	Feed-forward control	Flexible magnetic continuum robots	Cameras	Kidney phantom	N
Assisted urination <sup>[155]</sup>	Permanent cubic magnet	Predefined field apply	Magnetic soft robotic bladder	Computed tomography	Porcine bladder	Y

arteries, veins, and capillaries. Their diameters range from 25 mm for the aorta to 6  $\mu\text{m}$  for capillaries. In particular, large arteries have diameters ranging between 1 and 4 mm,<sup>[115]</sup> which is a crucial consideration for intervention applications. Furthermore, arteries are advantageous due to their deeper location within the muscle layers and thicker walls, making them an ideal intervention environment.

The successful use of endocardial catheters in medical interventions dates back to a decade.<sup>[117]</sup> Notably, the achievement of human cardiac interventions using magnetic catheters marked a

significant milestone in the field of magnetic steering, particularly in the treatment of atrial fibrillation ablation. Myocardial ablation surgery is one of the few applications that have been conducted in human trials. The surgery involves the use of a commercial MAS, named Stereotaxis Niobe, to control the direction of the magnetic catheter tip under fluoroscopic imaging. Other studies have documented related applications focusing on electrophysiological catheter guidance and control.<sup>[139,140]</sup> Subsequent research expanded to other heart diseases, including cardiac arrhythmias.<sup>[24]</sup>

Recent research efforts have been directed toward uncovering solutions for a range of diseases, including peripheral arterial diseases<sup>[131]</sup> and arterial aneurysms through on-demand embolization.<sup>[124]</sup> Microrobots were designed for active retention during drug delivery,<sup>[125]</sup> and a continuum magnetic robot was designed to enhance the access level.<sup>[113]</sup> In addition, the field of soft robotics has contributed to the exploration of soft magnetic manipulation systems,<sup>[141]</sup> wherein soft magnetic actuation introduces heightened flexibility in surgical procedures through remote magnetic control.

Peripheral arterial disease commonly occurs in people aged 40 years and above; it is caused by narrow blood vessels and can lead to pain, impaired walking, and claudication. Percutaneous endovascular intervention is the primary treatment option. The MAS is used to navigate the magnetic ring-tip catheter to an impaired location and then to place a stent or balloon to open the occluded vessel and restore the normal blood vessel diameter.<sup>[131]</sup> This system avoids X-ray radiation by remotely controlling the magnetic catheter, and localization is achieved through catheter-tip sensing. A cylindrical array of Hall effect sensors was designed to measure the magnetic flux density around the workspace, enabling the location of the magnetic catheter tip to be estimated. However, X-ray imaging is still required for the bifurcations. The proposed magnetic location estimation algorithm can estimate the location of the magnetic tip in real time. The proposed method has been applied using the Helmholtz coils to control the magnetic tip in the phantom.

Aneurysm is a malfunction that occurs in an artery and appears as an outward swelling or bulging in the blood vessel wall. This anomaly can manifest anywhere in the human body, often appearing in the aorta or the brain. Given their asymptomatic nature prior to an attack and the potential for severe internal bleeding upon rupture, aneurysms have a high fatality rate. Embolization is an effective strategy for the treatment of this condition. Therefore, an effective method for the magnetic-guided catheter-assisted delivery of microgels was proposed in ref. [124]. This method employs C-arm fluoroscopy for real-time imaging and uses a magnetic-based robotic arm for catheter guidance. The self-adhesive microgel delivered by the magnetic catheter was used as an embolic agent with an acidic stimulus to trigger the microgel connection. This innovative study demonstrated the feasibility of controlling a swarm of microrobots within a dynamic human body environment to achieve effective embolization. The proposed method was applied to an ex vivo human placenta to test its effectiveness. The effective embolization of the aneurysm under ultrasound imaging indicated that the microrobotic embolization platform is effective for human blood vessels.

Most applications inside blood vessels are under the tethered magnetic catheter because of the blood flow velocity. Navigating untethered microrobots within the bloodstream presents a central challenge for the swift flow of blood in the circulatory system. To overcome this hurdle, an ingenious solution involving an active retention structure<sup>[125]</sup> was developed. The microrobot was designed with a claw to maintain its position inside a blood vessel. This innovative mechanism ensures that the microrobots maintain their positions within the blood environment despite the vigorous blood flow. The successful implementation of this structure within a live rabbit jugular vein has opened the door to

applying untethered microrobot swarms in treating vascular diseases or drug delivery in the circulatory system using a noninvasive method.

Another approach to improve the ability of a tethered catheter is to design an untethered helical magnetic robot for improved endovascular access.<sup>[113]</sup> This new type of untethered robot was designed with an articulating magnetic tip structure to increase the ability of the robot to steer and a helical protrusion body to rotate the robot and generate the energy required to move forward. The system was also designed with a working channel at the center for fluid injection. X-ray radiography was used for real-time imaging of the position of the magnetic robot inside the vascular system. A commercial electromagnetic system, Navion, was used to control the magnetic robot. This electromagnetic actuation system achieved broad directional control of the catheter. An ex vivo experiment demonstrated the effectiveness of the helical structure in controlling the robot's forward movement. An ex vivo experiment using human placental blood vessels and an in vivo experiment using a porcine model demonstrated the effectiveness of the designed robot and system. A comparison of the live pig invasive study between the commercial and proposed catheters showed the effectiveness of the new design in moving backward without harming the vessels.

### 4.3. Intraocular System

In intraocular procedures, the surgeon's hand stability is paramount. Consequently, numerous research endeavors have been devoted to the design of mechanical systems to ensure a steady hand during surgery. Ex vivo tests conducted in chicken embryos and phantom models mimicking the human eye have contributed to this effort.<sup>[142,143]</sup> Moreover, the development of robotic arms aimed at mitigating surgeons' hand tremors has been pursued.<sup>[144]</sup>

Advancements in magnetically driven systems and controls have led to proposals for less invasive and more accessible solutions in the intraocular domain. In a study conducted in 2010, localization was achieved using a single camera, and experiments showed its effectiveness in a model eye.<sup>[145]</sup> This study laid the foundation for future intraocular surgeries. In subsequent research, an in vivo experiment on a rabbit eye further validated the potential for intraocular research.<sup>[146]</sup> A cylindrical microrobot with a diameter of 285  $\mu\text{m}$  and a length of 1.8 mm was developed to fit in a needle and be easily injected inside the eye. The Octomag was developed to perform surgery inside the eye with the MAS underneath, leaving a workspace for imaging and surgery in the front. Intraocular surgery holds a distinct advantage in imaging because of its exposure to the surface. However, the application is not ready for human trials because of problems related to uncontrollably fast motion when the system is used for drug delivery. In ocular globe material removal surgery, the force applied should be controlled accurately; therefore, its application is still in the animal trial stage. More recent research has focused on targeted therapy using rotating-gradient magnetic fields.<sup>[46]</sup> The successful implementation of this approach in bovine eyes underscores the capacity of magnetized microrobots propelled by preprogrammed magnetic fields for effective drug delivery in an intraocular environment.

#### 4.4. Knee and Elbow Joints

Cartilage damage to the knee and elbow joints is frequently observed in athletes and elderly individuals. Additionally, there has been a growing trend for such damage among younger people in recent years. The conventional approach to address this issue involves utilizing arthroscopy for imaging. Unfortunately, conventional medicine does not offer methods for the complete healing of the damaged cartilage. The primary treatment methods involve mitigating inflammation and extracting the joint fluid from the joint cavity to facilitate self-healing. The most advanced method, platelet-rich plasma (PRP) injection, is used to cure the early stages of damage. PRP injection involves supplying concentrated platelets to a damaged site to alleviate pain and expedite repair. However, the results of this method are not consistently remarkable, and variations in effectiveness exist among individuals.

An alternative solution that has long been proposed is the use of stem cells to treat serious injury to the cartilage. Mesenchymal stem cells (MSCs) can be readily sourced from the placental tissue or umbilical cord blood. This innovative approach involves loading MSCs onto porous microrobots, which are then injected into the affected joint through a needle and controlled by the MAS. Through magnetic navigation, precise medicine can be achieved. As documented in a study in 2020,<sup>[13]</sup> human adipose-derived MSCs can be used for knee cartilage regeneration. Experiments were conducted using a rabbit knee cartilage defect model. As the medical community increasingly embraces the stem cell theory for therapeutic applications, this approach holds significant potential for clinical implementation to cure damage inside human joints.

#### 4.5. Gastrointestinal System

Natural channels exist in the gastrointestinal system, and the space is relatively large. Therefore, it is considerably easier for a millirobot, capsule, or catheter to pass through this area. Endoscopy is necessary for patients with gastrointestinal malfunction. Colonoscopy, gastroscopy, and esophagoscopy are the corresponding diagnostic methods for different locations inside the human body, such as the intestines, stomach, or esophagus.

The classical research on video capsules actuated by Stereotaxis Niobe has been conducted using gastrointestinal endoscopy.<sup>[117]</sup> Controlling the position of a magnetic robot in a 3D environment is the key to endoscopy. The gastrointestinal system is relatively large compared with the intraocular system in 3D space; therefore, a large workspace is required for this application. Researchers tend to use robotic arm-based actuation systems and improved control methods to achieve large workspaces and accurate position control. A rotating actuator with a permanent magnet as an end effector was used to control the trajectory of the capsule endoscope.<sup>[80]</sup> In the following year, detailed research on a mock-up capsule controlled in a fluid-distended stomach with high robustness, such as a reduced control rate, localization rate, deviation of the applied field, and manipulation singularities, was conducted<sup>[81]</sup> to demonstrate the high potential of the robotic arm-based MAS and enhanced algorithm in clinical

practice. These two studies focused on the system design and algorithms to achieve complicated tasks. With the maturity of applications of capsule endoscopy in the gastrointestinal environment, further research tended to make improvements in magnetic actuation, such as at the autonomous<sup>[147]</sup> and cooperation levels.<sup>[148]</sup> In ref. [88], colonoscopy was studied specifically in terms of autonomy and intelligence. With an increase in the autonomous level, the cost of the test tended to be cheaper and more comfortable; therefore, the widespread application of gastrointestinal endoscopy would greatly benefit humans.

In recent years, microrobots have been proposed for stomach incision treatment, which is a new area of research on microrobot applications, with clinical trials still in the cell slice surface stage.<sup>[149]</sup> The main inspiration for this design was the rendering of the frictional anisotropy characteristic of the design of a microwalker to mimic walking. The most recent research also mentioned this type of design, called the asymmetrical friction effect, which is induced by magnetic torque.<sup>[150]</sup> Enhancing the magnetic robot design can significantly support the magnetic actuation method used in clinical practice. The emergence of applications in precise drug delivery and surgery assistance in the stomach demonstrates the maturity of the magnetic actuation technique and the corresponding control algorithm.

In addition to controlling a single microrobot to achieve tasks, the most recent research has been conducted using multiple microrobots.<sup>[151]</sup> Dynamic control of the magnetic field can achieve control of the soft film-like multilayer robot; the layers can be separated under a predefined magnetic field and fixed in separate locations to treat stomach ulcers. Such experiments were conducted on a porcine stomach to treat multiple ulcers.

#### 4.6. Respiratory System

The respiratory system encompasses the respiratory tract and lungs. The respiratory tract can be categorized into an upper portion (including the nose, mouth, pharynx, and throat) and a lower portion (consisting of the windpipe, bronchial tubes, and lungs). Although the upper respiratory tract components are relatively accessible, the lower respiratory tract, specifically the bronchial tubes and lungs, presents an intricate scenario. The following discussion primarily focuses on the complex areas of the respiratory system.

A position estimation method in which a lung phantom experiment was conducted was proposed.<sup>[152]</sup> In this approach, the key difficulty in controlling the endoscope in the lung is its positioning. Therefore, the image detected by the endoscope is used to obtain the current position of the catheter. The device kinematics were captured by comparing the applied input with visual feedback, which is a novel method for obtaining the position within the human lung structure in real time.

Bronchoscopy is a crucial technique for identifying diseases within the bronchial tubes. The development of an optimized navigation trajectory is imperative to enhance the navigation process for gentle and autonomous detection. This led to the creation of a soft magnetic-based catheter actuated by a cooperative arrangement of two robot-driven permanent magnets as actuators. This design aims to refine the navigation path for autonomous atraumatic detection within the bronchial tubes, as

highlighted by Pittiglio.<sup>[153]</sup> Autonomous detection of diseases within the bronchial tree phantom was achieved by deploying an optimally designed soft catheter robot. This innovation makes it possible to detect diseases in the bronchial tubes effectively, which can have far-reaching implications in medical diagnostics and interventions. This atraumatic autonomous endoscopy is achieved by the cooperation between two robotic arms to control a patient-specific magnetic catheter. The collaborative robotic arm is controlled to achieve a predefined trajectory for the catheter to demonstrate navigation with minimal contact. A comparative study was conducted between four catheters using a leader–follower algorithm proposed to control the catheter, and the tracking accuracy and targeting error were improved enormously.

#### 4.7. Urogenital System

The urogenital system comprises two distinct subdivisions: the urinary and genital tracts. The urinary tract encompasses essential components such as the kidney, ureter, bladder, and urethra. A prevalent ailment in the urogenital system is kidney stones. Retrograde intrarenal surgery serves as a method to remove these stones. The endoscope moves through the urine storage area and enters the kidney, identifies the stone, and breaks it with a laser.

Flexible magnetic continuum robots were developed for this application.<sup>[154]</sup> A catheter with a magnetic tip is implemented to navigate through the kidney phantom. The proposed control method can predict the continuum robot's nonlinear behavior under the heterogeneous magnetic field. Another application proposed in 2022 showed that a specially designed magnetic soft robotic bladder can enhance the contraction ability by increasing pressure through the magnetic actuation.<sup>[155]</sup> This novel application under magnetic actuation has paved the way for assisted urination. Its effectiveness was tested in a porcine model over a period of 2 weeks of implementation to certify its nontoxicity. The genital tract is categorized into two subcategories: the female and male reproductive systems. In the context of the male reproductive system, physical contraception is a notable application. Research in this domain has resulted in the development of wireless robots tailored for this purpose. Their potential has been demonstrated through the robots' application within a tubular phantom augmented by an ultrasound-guided system.<sup>[156]</sup>

## 5. Challenges and Opportunities

### 5.1. Development of MASs

The challenges of a sufficiently high magnetic field, high energy efficiency, a flexible and modular design, sufficient workspace, and a full DoF for controllability still exist and have not yet been solved in a single design. However, multiple solutions have been proposed to solve one of the aforementioned problems; some of these solutions can also solve other problems simultaneously.

Most state-of-the-art research on MAS design still focuses on the discrete wire method to elaborate on the model of electromagnet distribution. However, the design of the wrapping pattern should also be addressed. Special wrapping patterns, due to their ability to alter current density, have the potential to enhance the MAS performance significantly.<sup>[62]</sup> In addition to pattern

design, optimizing the parameters of mainstream MAS types is another area of focus.<sup>[19]</sup>

The da Vinci surgical robot concept can be extended to the remote manipulation of magnetized surgical instruments when the end effectors of the robotic arms are retrofitted with magnets. The permanent magnets exhibit a decrease in magnetic force and torque as they move further from the magnet, following the  $d^{-4}$  and  $d^{-3}$  relationships. This concept can emulate the effect of “turning off” when handling a permanent magnet away from the workspace. The electromagnets can be deactivated more easily by withdrawing current. The permanent and electromagnetic actuation systems can be integrated into the end effector of a robotic arm. Additionally, the more magnets a robotic-based system contains, the greater the flexibility and DoFs it can achieve. The collaboration of multiple robotic arms can achieve any configuration required, which would lead to great opportunities to improve flexible and modular designs during the development of MASs. The development of robotic arm-integrated systems is still in its early stages. Multiple configurations can be expected in future designs.

Despite the significant enhancements related to MAS design in recent years, achieving control over the 3D force and 3D heading of MMRs without encountering singularities remains challenging in terms of fully controlling the DoFs and having sufficient workspace. The current approach involves the use of movable electromagnets to create a changeable working area, such as motor-based<sup>[25]</sup> or robotic arm-based systems.<sup>[111]</sup> A trade-off solution should exist between having an appropriate workspace and achieving an effective magnetic-driven force or torque for specific applications. The integration of robotic arms with MASs as end effectors is the next major trend in clinical applications. High-gradient MASs with large controllable workspaces will continue to be the primary research direction in system design. Functionally enhanced MASs at low cost can be predicted for multiple clinical applications.

### 5.2. MMR and Controller Design

Although the controller design for robotic systems is relatively mature compared with MAS control, many practical problems exist, making it difficult to transfer these control methods to real-life situations under magnetic actuation, especially in complex in vivo environments. First, feedback information is difficult to obtain as accurately as in ex vivo experiments. Visual blocks and obstacles always exist in drug delivery or targeted treatment. Second, the size of the controlled objects affects the controller design. The characteristic of moving micro-/nano-objects is that the inertial forces can be neglected, and the viscous force is in the dominant position, which makes the movement of the MMR depend on the environment's viscosity. Third, changes in blood speed in the circulation system and individual differences complicate the controller design. Last but not least, feedback information detection, anything other than imaging, is also difficult because there are several device requirements or high calibration requirements. These challenges leave considerable room for controller applications and sensing system design improvements.

Compared with robotic applications in other medical fields, such as rehabilitation, the development of magnetic robots for

clinical practice is relatively slow. Several key challenges have contributed to this slow pace, including the size constraints of magnetic robots, their design at the clinical level, which needs to pass the Food and Drug Administration (FDA) examination, and their integration with real-time imaging and control. Additionally, magnetic robot motion analysis research is closely related to controller design research and is still in the high-speed development stage. In addition to these challenges, magnetic robot design also needs to consider its applicability to multiple clinical situations, nontoxicity, and biodegradability.

Imaging problems have resulted in a situation wherein the research focuses on control algorithms for MAS-controlled magnetic robots in clinical applications that primarily involve robots at the millimeter scale. However, as the materials for magnetic robots and imaging methods continue to evolve, it is anticipated that research on MAS-based control methods in clinical applications will gradually shift toward relatively larger robots before more compact and smaller robots following further advancements.

The integration of both the driving and sensing functions in a single microrobot presents significant challenges, and imaging can be particularly difficult. As a result, researchers have pursued an alternative approach, which involves using multiple microrobots suitable for imaging and control as well as forming a swarm or multiagent system. In such systems, it is essential to analyze the interaction forces generated between the microrobots and gain insight into other force mechanics. Numerous research endeavors are currently in progress, showing promise for future applications.

Owing to clinical application challenges, the microrobot design trend is shifting toward larger shapes to address control issues.<sup>[157]</sup> Enlarging microrobots to the millimeter scale can provide more realistic control for specific tasks. In terms of controller design, there has been a shift from open-loop control<sup>[126]</sup> to closed-loop real-time control<sup>[14]</sup> in vivo, from single-movement modes to multimodes,<sup>[158,159]</sup> and from single microrobots that reach a target and complete a task to multiple microrobots collaborating on a task.<sup>[20]</sup> Once these fundamental control-related challenges are addressed and improvements in microrobot manufacturing are achieved, clinical applications for specific surgeries will become more feasible.

In certain scenarios where obtaining imaging feedback is challenging, preprogrammed control remains a viable alternative for achieving effective control of microrobots. With advancements in magnetic field control, preprogrammed control may become an increasingly valuable substitute solution. For the control of untethered microrobots, swarm and multiagent systems with intelligent algorithms will continue to be the primary directions for control and modeling. The dynamic analysis of untethered MMRs inside complex fluid environments is also a promising research area for achieving accurate control with respect to different MMR structure designs. Systems utilizing magnet-tipped catheters will continue to be frequently employed in the context of tethered robotic control. The development of soft-continuum magnetic robots is also a promising direction.

### 5.3. Clinical Applications

Clinical applications have been under high-speed development in recent years. The clinical applications mentioned in

Section 4 represent recurring themes in contemporary cutting-edge research and practical implementation. However, the following challenges have been faced: the lack of human trials for most applications, realistic problems that exist during the transfer from the laboratory to the surgeon, and FDA approval for materials used in clinical trials. Depending on the urgency level of a disease, researchers tend to focus on diseases with a high level of urgency and neglect other applications, thereby leaving many opportunities for exploration. Unexplored or rarely explored applications, such as MMR delivery in the pancreas, cholecysts, livers, and reproductive systems, require further investigation. The primary application areas for MASs and their controls are the brain and the intravascular and gastrointestinal systems. Each application requires a specific MAS design, control, and magnetic robot design. To date, tethered robots have demonstrated easier clinical trials in humans than untethered robots. Most tethered robots used in human trials have been applied primarily in larger environments, such as the gastrointestinal system.

The imaging methods used mostly include conventional fluoroscopy and cameras to explore in vivo and ex vivo applications, whereas the optoacoustic tomography technique, although safer, is still in the animal trial stage. Tethered magnetic robotic solutions predominantly focus on magnetic catheters and endoscopes with permanent magnetic tips. Depending on the size of the application environment, untethered robots include millirobots, microrobots, and microrobot swarms. Preprogrammed control algorithms will continue to prevail in many applications. However, closed-loop control is increasingly utilized to perform specific tasks in the most advanced applications of robotic arm-based MASs. Similarly, in the context of MAS design, the traditional Helmholtz and permanent magnets with ball screws have been replaced by specially designed electromagnetic actuation systems and robotic arm-based actuation systems.

Broadly speaking, owing to their inherent attributes of being noninvasive and offering standard repeatability, robots used for medical purposes and operated via magnetically induced force continue to be a fertile ground for continued exploration and advancement.<sup>[160]</sup> This research trajectory is expected to persist in clinical research, underscoring the potential for innovative and impactful development in the years to come.

## 6. Conclusion

This review has explored the key research and techniques employed in MASs for clinical applications. In contrast to prior studies, this review has systematically addressed omitted yet critical topics. These encompass the evolution of MAS design and future research trends, a comprehensive analysis of the underlying principles of magnetic actuation, and the incorporation of commonly used analytical expressions for interdisciplinary researchers to gain a better understanding. Examples of clinical applications were presented in the system design section to illustrate the system designs required for specific medical applications. In the modeling and control aspects of MASs, the discussion revolved around general solutions with electromagnets functioning as actuators, aiming at providing readers with a swift grasp of the MMR control landscape. The control block

diagrams systematically illustrated the principles of controller design under magnetic actuation.

Additionally, the existing and potential applications within the human body were systematically analyzed, emphasizing their suitability for various purposes. The summary of clinical applications and the specific disease explanations can benefit researchers who are unfamiliar with the surgeries and diseases. The challenges and opportunities were summarized to provide broader insights. From the authors' perspective, future research trends will increasingly center on designing portable MASs with expansive workspaces, creating biodegradable MMRs, and advancing toward clinical trials. One critical problem is that the techniques have been developing in their own fields, and only a few are aimed at interdisciplinary areas to solve problems in the gap area. To address this situation, research should focus on combining all these techniques at the frontier and building systemic solutions. In conclusion, this field holds significant potential and offers substantial benefits for modern medicine, underlying considerable opportunities in both academic and commercial fields.

## Acknowledgements

This work was supported in part by National Key Research and Development Project of China under grant 2023YFB4705300; in part by National Natural Science Foundation of China (NSFC-SRI) R-IND13303 and grant U22A2064; in part by the InnoHK Project on Project 2.6 at Hong Kong Centre for Cerebro-cardiovascular Health Engineering (COCHE); in part by Hong Kong Collaborative Research Fund CRF 8730059; in part by the Shenzhen Science and Technology Program under grant JCYJ20220818101611025, Grant RCJC20231211085926038; in part by the Guangdong Basic and Applied Basic Research Foundation (2022B1515120010); in part by SIAT-CUHK Joint Laboratory of Robotics and Intelligent Systems; in part by Research Institute for Advanced Manufacturing (no. 1-CD9F and 1-CDK3); and the Startup fund (no. 1-BE9L), The Hong Kong Polytechnic University.

## Conflict of Interest

The authors declare no conflict of interest.

## Keywords

magnetic robots, magnetic actuation systems, control, clinical applications

Received: May 21, 2024

Revised: June 16, 2024

Published online: August 11, 2024

- [1] R. Diekmann, D. L. Wolfson, C. Spahn, M. Heilemann, M. Schüttel, T. Huser, *Nat. Commun.* **2016**, *7*, 13711.
- [2] M. Xie, A. Shakoor, Y. Shen, J. K. Mills, D. Sun, *IEEE Trans. Biomed. Eng.* **2018**, *66*, 199.
- [3] Y. Deng, A. Paskert, Z. Zhang, R. Wittkowski, D. Ahmed, *Sci. Adv.* **2023**, *9*, eadh5260.
- [4] A. Aghakhani, O. Yasa, P. Wrede, M. Sitti, *Proc. Natl. Acad. Sci.* **2020**, *117*, 3469.
- [5] S. Sánchez, L. Soler, J. Katuri, *Angew. Chem., Int. Ed.* **2015**, *54*, 1414.

- [6] A. A. Solovov, Y. Mei, E. Bermúdez Ureña, G. Huang, O. G. Schmidt, *Small* **2009**, *5*, 1688.
- [7] G. Kosa, P. Hunziker, *Adv. Intell. Syst.* **2019**, *1*, 1900035.
- [8] L. Daneshmandi, S. Shah, T. Jafari, M. Bhattacharjee, D. Momah, N. Saveh-Shemshaki, K. W. Lo, C. T. Laurencin, *Trends Biotechnol.* **2020**, *38*, 1373.
- [9] D. Shi, X. Xu, Y. Ye, K. Song, Y. Cheng, J. Di, Q. Hu, J. Li, H. Ju, Q. Jiang, Z. Gu, *ACS Nano* **2016**, *10*, 1292.
- [10] T. D. Bornes, A. B. Adesida, N. M. Jomha, *Arthritis Res. Ther.* **2014**, *16*, 1.
- [11] J. Li, X. Li, T. Luo, R. Wang, C. Liu, S. Chen, D. Li, J. Yue, S.-H. Cheng, D. Sun, *Sci. Robot.* **2018**, *3*, eaat8829.
- [12] T. Wei, J. Liu, D. Li, S. Chen, Y. Zhang, J. Li, L. Fan, Z. Guan, C.-M. Lo, L. Wang, K. Man, D. Sun, *Small* **2020**, *16*, 1906908.
- [13] G. Go, S.-G. Jeong, A. Yoo, J. Han, B. Kang, S. Kim, K. T. Nguyen, Z. Jin, C.-S. Kim, Y. R. Seo, J. Y. Kang, J. Y. Na, E. K. Song, Y. Jeong, J. K. Seon, J.-O. Park, E. Choi, *Sci. Robot.* **2020**, *5*, eaay6626.
- [14] L. Zheng, Y. Jia, D. Dong, W. Lam, D. Li, H. Ji, D. Sun, *IEEE Trans. Robot.* **2022**, *38*, 1583.
- [15] D. Dong, L. Xing, L. Zheng, Y. Jia, D. Sun, *IEEE Trans. Control Syst. Technol.* **2021**, *30*, 1.
- [16] M. S. Grady, M. A. Howard III, J. A. Molloy, R. C. Ritter, E. G. Quate, G. T. Gillies, *Med. Phys.* **1990**, *17*, 405.
- [17] J. Nam, W. Lee, E. Jung, G. Jang, *IEEE Trans. Ind. Electron.* **2017**, *65*, 5673.
- [18] Q. Boehler, S. Gervasoni, S. L. Charreyron, C. Chautems, B. J. Nelson, *IEEE Trans. Robot.* **2023**, *39*, 791.
- [19] L. Yang, Z. Yang, M. Zhang, J. Jiang, H. Yang, L. Zhang, *IEEE Trans. Autom. Sci. Eng.* **2022**, *1*.
- [20] H. Xie, M. Sun, X. Fan, Z. Lin, W. Chen, L. Wang, L. Dong, Q. He, *Sci. Robot.* **2019**, *4*, eaav8006.
- [21] S. R. Goudou, I. C. Yasa, X. Hu, H. Ceylan, W. Hu, M. Sitti, *Adv. Funct. Mater.* **2020**, *30*, 2004975.
- [22] D. Ahmed, A. Sukhov, D. Hauri, D. Rodrigue, G. Maranta, J. Harting, B. J. Nelson, *Nat. Mach. Intell.* **2021**, *3*, 116.
- [23] X. Yang, R. Tan, H. Lu, T. Fukuda, Y. Shen, *Nat. Commun.* **2022**, *13*, 4156.
- [24] J. Liu, Q. Wang, H. Wang, Y. Li, X. Hu, J. Cheng, Y. Dai, *IEEE Trans. Appl. Supercond.* **2016**, *26*, 1.
- [25] F. Ongaro, S. Pane, S. Scheggi, S. Misra, *IEEE Trans. Robot.* **2019**, *35*, 174.
- [26] L. Yang, X. Du, E. Yu, D. Jin, L. Zhang, in *2019 Inter. Conf. on Robotics and Automation (ICRA)*, **2019**, pp. 9814–9820.
- [27] Z. Li, Z. Lin, S. Liu, H. Yagi, X. Zhang, L. Yocum, M. Romero-Lopez, C. Rhee, M. J. Makarczyk, I. Yu, E. N. Li, M. R. Fritch, Q. Gao, K. B. Goh, B. O'Donnell, T. Hao, P. G. Alexander, B. Mahadik, J. P. Fisher, S. B. Goodman, B. A. Bunnell, R. S. Tuan, H. Lin, *Adv. Sci.* **2022**, *9*, 2105909.
- [28] P. Wrede, O. Degtyaruk, S. K. Kalva, X. L. Deán-Ben, U. Bozuyuk, A. Aghakhani, B. Akolpoglu, M. Sitti, D. Razansky, *Sci. Adv.* **2022**, *8*, eabm9132.
- [29] A. C. Bakenecker, A. von Gladiss, T. Friedrich, U. Heinen, H. Lehr, K. Lütke-Buzug, T. M. Buzug, *J. Magn. Magn. Mater.* **2019**, *473*, 495.
- [30] D. Son, S. Yim, M. Sitti, *IEEE/ASME Trans. Mechatron.* **2015**, *21*, 708.
- [31] M. G. Christiansen, L. R. Stöcklin, C. Forbrigger, S. A. Venkatesh, S. Schuerle, *PNAS Nexus* **2023**, *2*, pgad297.
- [32] B. Gleich, I. Schmale, T. Nielsen, J. Rahmer, *Science* **2023**, *380*, 966.
- [33] E. Diller, J. Giltinan, M. Sitti, *Int. J. Robot. Res.* **2013**, *32*, 614.
- [34] D. Loghin, C. Tremblay, M. Mohammadi, S. Martel, *Int. J. Robot. Res.* **2017**, *36*, 1195.
- [35] Q. Wang, L. Zhang, *ACS Nano* **2021**, *15*, 149.
- [36] J. Yu, L. Yang, L. Zhang, *Int. J. Robot. Res.* **2018**, *37*, 912.

- [37] L. Yang, J. Jiang, X. Gao, Q. Wang, Q. Dou, L. Zhang, *Nat. Mach. Intell.* **2022**, 4, 480.
- [38] B. E. Kratochvil, M. P. Kummer, J. J. Abbott, R. Borer, O. Ergeneman, B. J. Nelson, in *2010 IEEE Inter. Conf. on Robotics and Automation (ICRA)*, IEEE, Piscataway, NJ **2010**, pp. 1080–1081.
- [39] P. G. Huray, *Maxwell's Equations*, John Wiley & Sons, Hoboken, NJ **2011**.
- [40] A. J. Petruska, A. W. Mahoney, J. J. Abbott, *IEEE Trans. Robot.* **2014**, 30, 1222.
- [41] A. J. Petruska, J. J. Abbott, *IEEE Trans. Magn.* **2013**, 49, 811.
- [42] P. Ryan, E. Diller, *IEEE Trans. Robot.* **2017**, 33, 1398.
- [43] E. Diller, J. Giltinan, G. Z. Lum, Z. Ye, M. Sitti, *Int. J. Robot. Res.* **2016**, 35, 114.
- [44] M. Parker, *Nat. Electron.* **2021**, 4, 770.
- [45] B. Shapiro, S. Kulkarni, A. Nacev, S. Muro, P. Y. Stepanov, I. N. Weinberg, *Wiley Interdiscip. Rev.: Nanomed. Nanobiotechnol.* **2015**, 7, 446.
- [46] L. Xing, D. Li, H. Cao, L. Fan, L. Zheng, L. Zhang, D. Sun, *Adv. Intell. Syst.* **2022**, 4, 2100214.
- [47] H. Xie, X. Fan, M. Sun, Z. Lin, Q. He, L. Sun, *IEEE/ASME Trans. Mechatron.* **2019**, 24, 902.
- [48] J. Rahmer, C. Stehning, B. Gleich, *Sci. Robot.* **2017**, 2, eaal2845.
- [49] J. Law, X. Wang, M. Luo, L. Xin, X. Du, W. Dou, T. Wang, G. Shan, Y. Wang, P. Song, X. Huang, J. Yu, Y. Sun, *Sci. Adv.* **2022**, 8, eabm5752.
- [50] F. Niu, W. Ma, X. Li, H. K. Chu, J. Yang, H. Ji, D. Sun, in *14th IEEE Inter. Conf. on Nanotechnology*, IEEE, Piscataway, NJ **2014**, pp. 127–130.
- [51] F. Niu, J. Li, W. Ma, J. Yang, D. Sun, *IEEE/ASME Trans. Mechatron.* **2017**, 22, 2265.
- [52] Y. Xing, Y. Jia, Z. Zhan, J. Li, C. Hu, in *2021 IEEE Inter. Conf. on Robotics and Automation (ICRA)*, IEEE, Piscataway, NJ **2021**, pp. 7281–7287.
- [53] P. Liao, L. Xing, S. Zhang, D. Sun, *Small* **2019**, 15, 1901197.
- [54] T. W. Fountain, P. V. Kailat, J. J. Abbott, in *2010 IEEE Inter. Conf. on Robotics and Automation (ICRA)*, IEEE, Piscataway, NJ **2010**, pp. 576–581.
- [55] R. Avaneesh, R. Venezian, C.-S. Kim, J.-O. Park, S. Misra, I. S. Khalil, in *2021 IEEE/RSJ Inter. Conf. on Intelligent Robots and Systems (IROS)*, IEEE, Piscataway, NJ **2021**, pp. 8545–8550.
- [56] J. J. Abbott, E. Diller, A. J. Petruska, *Annu. Rev. Control Robot. Auton. Syst.* **2020**, 3, 57.
- [57] T. Xu, G. Hwang, N. Andreff, S. Régnier, *IEEE Trans. Robot.* **2015**, 31, 117.
- [58] H. Choi, K. Cha, S. Jeong, J.-O. Park, S. Park, *IEEE/ASME Trans. Mechatron.* **2012**, 18, 1221.
- [59] G. B. Jang, S. Jeon, J. Nam, W. Lee, G. Jang, *IEEE Trans. Magn.* **2015**, 51, 1.
- [60] G. Go, H. Choi, S. Jeong, C. Lee, S. Y. Ko, J.-O. Park, S. Park, *IEEE Trans. Magn.* **2015**, 51, 1.
- [61] S. S. Hidalgo-Tobon, *Concept. Magn. Reson., Part A* **2010**, 36, 223.
- [62] H. Pan, F. Jia, Z.-Y. Liu, M. Zaitsev, J. Hennig, J. G. Korvink, *Chin. Phys. B* **2018**, 27, 050201.
- [63] C. Yu, J. Kim, H. Choi, J. Choi, S. Jeong, K. Cha, J.-O. Park, S. Park, *Sens. Actuators, A* **2010**, 161, 297.
- [64] A. Heilbronn, *Jahrb. Wiss. Bot.* **1922**, 61, 284.
- [65] R. Eisenschitz, W. Philippoff, *Naturwissenschaften* **1933**, 21, 527.
- [66] W. Zhang, Y. Meng, P. Huang, *IEEE Trans. Magn.* **2008**, 44, 2367.
- [67] C. Watson, T. K. Morimoto, *IEEE Robot. Autom. Lett.* **2020**, 5, 2666.
- [68] M. Hagiwara, T. Kawahara, Y. Yamanishi, F. Arai, *Appl. Phys. Lett.* **2010**, 97, 013701.
- [69] J. S. Barajas-Gamboa, F. Huidobro, J. Jensen, R. Luengas, J. Rodriguez, C. Abril, R. Corcelles, M. Kroh, *Int. J. Med. Robot. Comput. Assist. Surg.* **2021**, 17, 1.
- [70] X. Du, M. Zhang, J. Yu, L. Yang, P. W. Y. Chiu, L. Zhang, *IEEE/ASME Trans. Mechatron.* **2020**, 26, 1524.
- [71] X. Du, Q. Wang, D. Jin, P. W. Y. Chiu, C. P. Pang, K. K. L. Chong, L. Zhang, *IEEE Robot. Autom. Lett.* **2022**, 7, 7668.
- [72] R. D. Brewer, K. E. Loewke, E. F. Duval, J. K. Salisbury, in *2008 2nd IEEE RAS EMBS Inter. Conf. on Biomedical Robotics and Biomechatronics*, IEEE, Piscataway, NJ **2008**, pp. 580–586.
- [73] E. Edelman, J. Kost, H. Bobeck, R. Langer, *J. Biomed. Mater. Res.* **1985**, 19, 67.
- [74] H. Yu, W. Tang, G. Mu, H. Wang, X. Chang, H. Dong, L. Qi, G. Zhang, T. Li, *Micromachines* **2018**, 9, 540.
- [75] L. Zhang, J. J. Abbott, L. Dong, B. E. Kratochvil, D. Bell, B. J. Nelson, *Appl. Phys. Lett.* **2009**, 94, 064107.
- [76] U. K. Cheang, D. Roy, J. H. Lee, M. J. Kim, *Appl. Phys. Lett.* **2010**, 97, 213704.
- [77] T. Li, A. Zhang, G. Shao, M. Wei, B. Guo, G. Zhang, L. Li, W. Wang, *Adv. Funct. Mater.* **2018**, 28, 1706066.
- [78] N. M. Shupak, F. S. Prato, A. W. Thomas, *URSI Radio Sci. Bull.* **2003**, 2003, 9.
- [79] M. Kobayashi, A. Pascual-Leone, *Lancet Neurol.* **2003**, 2, 145.
- [80] A. W. Mahoney, J. J. Abbott, *IEEE Trans. Robot.* **2014**, 30, 411.
- [81] A. W. Mahoney, J. J. Abbott, *Int. J. Robot. Res.* **2016**, 35, 129.
- [82] I. S. Khalil, A. Alfar, A. F. Tabak, A. Klingner, S. Stramigioli, M. Sitti, in *2017 IEEE Inter. Conf. on Advanced Intelligent Mechatronics (AIM)*, IEEE, Piscataway, NJ **2017**, pp. 1117–1122.
- [83] G. Pittiglio, M. Brockdorff, T. da Veiga, J. Davy, J. H. Chandler, P. Valdastrì, *IEEE Trans. Robot.* **2023**, 39, 1407.
- [84] H. Choi, J. Choi, G. Jang, J.-O. Park, S. Park, *Smart Mater. Struct.* **2009**, 18, 055007.
- [85] J. Rahmer, C. Stehning, B. Gleich, *PLoS One* **2018**, 13, e0193546.
- [86] A. J. Petruska, B. J. Nelson, *IEEE Trans. Robot.* **2015**, 31, 714.
- [87] M. S. Poole, Ph.D. dissertation, University of Nottingham, **2007**.
- [88] J. W. Martin, B. Scaglioni, J. C. Norton, V. Subramanian, A. Arezzo, K. L. Obstein, P. Valdastrì, *Nat. Mach. Intell.* **2020**, 2, 595.
- [89] E. Morita, N. Ohtsuka, Y. Shindo, S. Nouda, T. Kuramoto, T. Inoue, M. Murano, E. Umegaki, K. Higuchi, *Gastrointest. Endosc.* **2010**, 72, 836.
- [90] P. Liao, J. Li, S. Zhang, D. Sun, in *2018 IEEE Inter. Conf. on Robotics and Automation (ICRA)*, IEEE, Piscataway, NJ **2018**, pp. 3581–3586.
- [91] L. Wang, H. Xu, W. Zhai, B. Huang, W. Rong, *J. Bionic Eng.* **2017**, 14, 26.
- [92] D. Li, M. Jeong, E. Oren, T. Yu, T. Qiu, *Robotics* **2019**, 8, 87.
- [93] J. J. Abbott, K. E. Peyer, M. C. Lagomarsino, L. Zhang, L. Dong, I. K. Kaliakatsos, B. J. Nelson, *Int. J. Robot. Res.* **2009**, 28, 1434.
- [94] I. Buttinoni, J. Bialké, F. Kümmel, H. Löwen, C. Bechinger, T. Speck, *Phys. Rev. Lett.* **2013**, 110, 238301.
- [95] F. Ma, S. Wang, D. T. Wu, N. Wu, *Proc. Natl. Acad. Sci.* **2015**, 112, 6307.
- [96] S. Hernández-Navarro, P. Tierno, J. A. Farrera, J. Ignés-Mullol, F. Sagués, *Angew. Chem. Int. Ed.* **2014**, 53, 10 696.
- [97] A. Kaiser, A. Snezhko, I. S. Aranson, *Sci. Adv.* **2017**, 3, e1601469.
- [98] A. Bricard, J.-B. Caussin, N. Desreumaux, O. Dauchot, D. Bartolo, *Nature* **2013**, 503, 95.
- [99] F. Martínez-Pedrero, A. Ortiz-Ambríz, I. Pagonabarraga, P. Tierno, *Phys. Rev. Lett.* **2015**, 115, 138301.
- [100] H. Massana-Cid, F. Martínez-Pedrero, E. Navarro-Argem, I. Pagonabarraga, P. Tierno, *New J. Phys.* **2017**, 19, 103031.
- [101] G. Kokot, A. Snezhko, *Nat. Commun.* **2018**, 9, 1.
- [102] J. Yu, B. Wang, X. Du, Q. Wang, L. Zhang, *Nat. Commun.* **2018**, 9, 3260.
- [103] T. Xu, C. Huang, Z. Lai, X. Wu, *IEEE Trans. Robot.* **2022**, 38, 2875.
- [104] S. Floyd, E. Diller, C. Pawashe, M. Sitti, *Int. J. Robot. Res.* **2011**, 30, 1553.

- [105] E. Diller, S. Floyd, C. Pawashe, M. Sitti, *IEEE Trans. Robot.* **2011**, *28*, 172.
- [106] E. Diller, M. Sitti, *Adv. Funct. Mater.* **2014**, *24*, 4397.
- [107] M. Medina-Sánchez, V. Magdanz, M. Guix, V. M. Fomin, O. G. Schmidt, *Adv. Funct. Mater.* **2018**, *28*, 1707228.
- [108] K. Yesin, K. Vollmers, B. Nelson, in *2004 IEEE Inter. Conf. on Robotics and Automation (ICRA)*, IEEE, Piscataway, NJ **2004**, Vol. 2, pp. 1333–1338.
- [109] D. Meeker, E. Maslen, R. Ritter, F. Creighton, *IEEE Trans. Magn.* **1996**, *32*, 320.
- [110] P. Berkelman, M. Dzadovsky, *IEEE/ASME Trans. Mechatron.* **2011**, *18*, 44.
- [111] J. Sikorski, C. M. Heunis, F. Franco, S. Misra, *IEEE Trans. Magn.* **2019**, *55*, 1.
- [112] X. Liu, L. Wang, Y. Xiang, F. Liao, N. Li, J. Li, J. Wang, Q. Wu, C. Zhou, Y. Yang, H. Tang, N. Zhou, C. Wan, Z. Yin, G.-Z. Yang, G. Tao, J. Zang, *Sci. Robot.* **2024**, *9*, eadh2479.
- [113] R. Dreyfus, Q. Boehler, S. Lyttle, P. Gruber, J. Lussi, C. Chautems, S. Gervasoni, J. Berberat, D. Seibold, N. Ochsenbein-Köible, M. Reinehr, M. Weisskopf, L. Remonda, B. J. Nelson, *Sci. Robot.* **2024**, *9*, eadh0298.
- [114] K. B. Yesin, K. Vollmers, B. J. Nelson, *Int. J. Robot. Res.* **2006**, *25*, 527.
- [115] J.-B. Mathieu, G. Beaudoin, S. Martel, *IEEE Trans. Biomed. Eng.* **2006**, *53*, 292.
- [116] G. Gillies, R. Ritter, W. Broaddus, M. Grady, M. Howard III, R. McNeil, *Rev. Sci. Instrum.* **1994**, *65*, 533.
- [117] F. Carpi, C. Pappone, *Expert Rev. Med. Devices* **2009**, *6*, 487.
- [118] B. L. Nguyen, J. L. Merino, E. S. Gang, *Eur. Cardiol.* **2010**, *6*, 50.
- [119] R. Robbins, Redundant PLC controls heart-mapping machine, pp. 20–21, **2010**.
- [120] F. Kiemeneij, M. S. Patterson, G. Amoroso, G. Laarman, T. Slagboom, *Catheter. Cardiovasc. Interv.* **2008**, *71*, 510.
- [121] C. Chautems, B. J. Nelson, in *2017 IEEE Inter. Conf. on Robotics and Automation (ICRA)*, IEEE, Piscataway, NJ **2017**, pp. 4837–4842.
- [122] C. Chautems, B. Zeydan, S. Charreyron, G. Chatzipirpiridis, S. Pané, B. J. Nelson, *Eur. J. Cardio-Thorac. Surg.* **2017**, *51*, 405.
- [123] D. Son, M. C. Ugurlu, M. Sitti, *Sci. Adv.* **2021**, *7*, eabi8932.
- [124] D. Jin, Q. Wang, K. F. Chan, N. Xia, H. Yang, Q. Wang, S. C. H. Yu, L. Zhang, *Sci. Adv.* **2023**, *9*, eadf9278.
- [125] T. Li, S. Yu, B. Sun, Y. Li, X. Wang, Y. Pan, C. Song, Y. Ren, Z. Zhang, K. T. Grattan, Z. Wu, J. Zhao, *Sci. Adv.* **2023**, *9*, eadg4501.
- [126] A. J. Petruska, *IEEE Robot. Autom. Lett.* **2020**, *5*, 5472.
- [127] X. Fan, X. Dong, A. C. Karacakol, H. Xie, M. Sitti, *Proc. Natl. Acad. Sci.* **2020**, *117*, 27 916.
- [128] Q. Zou, X. Du, Y. Liu, H. Chen, Y. Wang, J. Yu, *IEEE Trans. Autom. Sci. Eng.* **2022**, *1*.
- [129] L. Huang, L. Rogowski, M. J. Kim, A. T. Becker, in *2017 IEEE/RSJ Inter. Conf. on Intelligent Robots and Systems (IROS)*, IEEE, Piscataway, NJ **2017**, pp. 414–420.
- [130] M. Salehizadeh, E. D. Diller, *IEEE Robot. Autom. Lett.* **2021**, *6*, 2674.
- [131] J. Wu, K. Yu, I. Lopez, A. A. Izquierdo, H. Saber, F. Alambeigi, L. Zhou, *IEEE Robot. Autom. Lett.* **2023**, *8*, 5656.
- [132] J. Liu, T. Xu, X. Wu, *IEEE Trans. Autom. Sci. Eng.* **2023**, *20*, 1577.
- [133] J. Jiang, L. Yang, L. Zhang, *IEEE Robot. Autom. Lett.* **2021**, *6*, 827.
- [134] A. Komae, B. Shapiro, *IEEE Trans. Control Syst. Technol.* **2011**, *20*, 1011.
- [135] S. O. Demir, U. Culha, A. C. Karacakol, A. Pena-Francesch, S. Trimpe, M. Sitti, *Int. J. Robot. Res.* **2021**, *40*, 1331.
- [136] J. Liu, X. Wu, C. Huang, L. Manamanchaiyaporn, W. Shang, X. Yan, T. Xu, *IEEE Trans. Autom. Sci. Eng.* **2020**, *18*, 1380.
- [137] T. Xu, J. Liu, C. Huang, T. Sun, X. Wu, *IEEE Trans. Autom. Sci. Eng.* **2021**, *19*, 2267.
- [138] L. Yang, J. Yu, L. Zhang, in *2020 IEEE Inter. Conf. on Robotics and Automation (ICRA)*, IEEE, Piscataway, NJ **2020**, pp. 9230–9236.
- [139] V. N. Le, N. H. Nguyen, K. Alameh, R. Weerasooriya, P. Pratten, *Med. Phys.* **2016**, *43*, 650.
- [140] E. S. Gang, B. L. Nguyen, Y. Shachar, L. Farkas, L. Farkas, B. Marx, D. Johnson, M. C. Fishbein, C. Gaudio, S. J. Kim, *Circ.: Arrhythm. Electrophysiol.* **2011**, *4*, 770.
- [141] M. Richter, M. Kaya, J. Sikorski, L. Abelmann, V. Kalpathy Venkiteswaran, S. Misra, *Soft Robot.* **2023**.
- [142] C. N. Riviere, W. T. Ang, P. K. Khosla, *IEEE Trans. Robot. Autom.* **2003**, *19*, 793.
- [143] B. Mitchell, J. Koo, I. Iordachita, P. Kazanzides, A. Kapoor, J. Handa, G. Hager, R. Taylor, in *Proc. 2007 IEEE Inter. Conf. on Robotics and Automation (ICRA)*, IEEE, Piscataway, NJ **2007**, pp. 623–629.
- [144] W. Wei, R. E. Goldman, H. F. Fine, S. Chang, N. Simaan, *IEEE Trans. Robot.* **2008**, *25*, 147.
- [145] C. Bergeles, K. Shamaei, J. J. Abbott, B. J. Nelson, *IEEE Trans. Biomed. Eng.* **2010**, *57*, 2064.
- [146] F. Ullrich, C. Bergeles, J. Pokki, O. Ergeneman, S. Erni, G. Chatzipirpiridis, S. Pané, C. Framme, B. J. Nelson, *Invest. Ophthalmol. Vis. Sci.* **2013**, *54*, 2853.
- [147] Y. Xu, K. Li, Z. Zhao, M. Q.-H. Meng, *IEEE Robot. Autom. Lett.* **2022**, *7*, 1729.
- [148] S. Kim, S. Bae, W. Lee, G. Jang, *IEEE Trans. Ind. Electron.* **2024**, *71*, 739.
- [149] Y. Jia, P. Liao, Y. Wang, D. Sun, *Adv. Intell. Syst.* **2022**, *4*, 2200118.
- [150] J. Zhao, C. Xin, J. Zhu, N. Xia, B. Hao, X. Liu, Y. Tan, S. Yang, X. Wang, J. Xue, Q. Wang, H. Lu, L. Zhang, *Adv. Mater.* **2024**, *36*, 2312655.
- [151] Z. Chen, Y. Wang, H. Chen, J. Law, H. Pu, S. Xie, F. Duan, Y. Sun, N. Liu, J. Yu, *Nat. Commun.* **2024**, *15*, 644.
- [152] J. Edelmann, A. J. Petruska, B. J. Nelson, *J. Med. Robot. Res.* **2018**, *3*, 1850002.
- [153] G. Pittiglio, P. Lloyd, T. da Veiga, O. Onaizah, C. Pompili, J. H. Chandler, P. Valdastris, *Soft Robot.* **2022**, *9*, 1120.
- [154] D. Lin, J. Wang, N. Jiao, Z. Wang, L. Liu, *Adv. Intell. Syst.* **2021**, *3*, 2000211.
- [155] Y. Yang, J. Wang, L. Wang, Q. Wu, L. Ling, Y. Yang, S. Ning, Y. Xie, Q. Cao, L. Li, J. Liu, Q. Ling, J. Zang, *Sci. Adv.* **2022**, *8*, eabq1456.
- [156] T. Wang, W. Hu, Z. Ren, M. Sitti, *IEEE Robot. Autom. Lett.* **2020**, *5*, 4859.
- [157] H. McClintock, F. Z. Temel, N. Doshi, J.-S. Koh, R. J. Wood, *Sci. Robot.* **2018**, *3*, eaar3018.
- [158] S. Yu, T. Li, F. Ji, S. Zhao, K. Liu, Z. Zhang, W. Zhang, Y. Mei, *Mater. Today Adv.* **2022**, *14*, 100231.
- [159] X. Yan, Q. Zhou, M. Vincent, Y. Deng, J. Yu, J. Xu, T. Xu, T. Tang, L. Bian, Y.-X. J. Wang, K. Kostarelos, L. Zhang, *Sci. Robot.* **2017**, *2*, eaaq1155.
- [160] B. J. Nelson, S. Gervasoni, P. W. Chiu, L. Zhang, A. Zemmar, *Proc. IEEE* **2022**, *110*, 1028.
- [161] X. Li, C. Lu, Z. Song, W. Ding, X.-P. Zhang, *IEEE Robot. Autom. Lett.* **2022**, *7*, 9264.
- [162] D. Li, F. Niu, J. Li, X. Li, D. Sun, *IEEE Trans. Ind. Electron.* **2020**, *67*, 4700.
- [163] P. Valdastris, E. Sinibaldi, S. Caccavaro, G. Tortora, A. Menciassi, P. Dario, *IEEE Trans. Robot.* **2011**, *27*, 769.
- [164] A. W. Mahoney, D. L. Cowan, K. M. Miller, J. J. Abbott, in *2012 IEEE Inter. Conf. on Robotics and Automation*, IEEE, Piscataway, NJ **2012**, pp. 3375–3380.
- [165] A. W. Mahoney, S. E. Wright, J. J. Abbott, in *2013 IEEE Inter. Conf. on Robotics and Automation*, IEEE, Piscataway, NJ **2013**, pp. 5366–5371.

- [166] S. E. Wright, A. W. Mahoney, K. M. Popek, J. J. Abbott, *IEEE Trans. Robot.* **2017**, *33*, 1013.
- [167] L. Yang, M. Zhang, Z. Yang, H. Yang, L. Zhang, in *2023 IEEE Inter. Conf. on Robotics and Automation (ICRA)*, IEEE, Piscataway, NJ **2023**, pp. 4696–4702.
- [168] G. Pittiglio, A. L. Orekhov, T. da Veiga, S. Calò, J. H. Chandler, N. Simaan, P. Valdastri, *IEEE Robot. Autom. Lett.* **2023**, *8*, 3980.
- [169] T. da Veiga, G. Pittiglio, M. Brockdorff, J. H. Chandler, P. Valdastri, *IEEE Robot. Autom. Lett.* **2023**, *8*, 3422.
- [170] K. Abolfathi, J. A. Rosales-Medina, H. Khaksar, J. H. Chandler, K. D. McDonald-Maier, K. Ashkan, P. Valdastri, A. K. Hoshiar, *IEEE Robot. Autom. Lett.* **2023**, *8*, 4235.
- [171] J. Davy, T. Da Veiga, G. Pittiglio, J. H. Chandler, P. Valdastri, in *2023 Inter. Symp. on Medical Robotics (ISMR)*, IEEE, Piscataway, NJ **2023**, pp. 1–7.
- [172] J. Lee, H. M. Cuong, J. Kim, E. Choi, H. Kee, S. Yang, J.-O. Park, S. Park, in *2023 IEEE/RSJ Inter. Conf. on Intelligent Robots and Systems (IROS)*, IEEE, Piscataway, NJ **2023**, pp. 2628–2634.
- [173] M. C. Hoang, S. Liu, K. T. Nguyen, H.-S. Lee, A. Hong, S. Bang, J. Kim, J.-O. Park, C.-S. Kim, *Sens. Actuators, A* **2023**, *361*, 114596.
- [174] H. Wang, J. Cui, K. Tian, Y. Han, *Nat. Commun.* **2023**, *14*, 7491.
- [175] C. J. Zimmermann, A. J. Petruska, K. B. Neeves, D. W. Marr, *Adv. Intell. Syst.* **2023**, *5*, 2300332.



**Yingxin Huo** received her master's degree from the Hong Kong University of Science and Technology in 2017. She was an assistant research fellow with the Department of Mechanical and Automation Engineering, the Chinese University of Hong Kong after graduation. She has been a PhD candidate with the City University of Hong Kong, Kowloon, Hong Kong, since 2020. Her research interests include the design and control of robotic systems, robotics and automation, and human-robot interaction. She published multiple papers in top journals and conferences as the first author and served as a reviewer for TIE, TMECH, TCST, TASE, and IROS.



**Lidong Yang** received his Ph.D. in mechanical and automation engineering from The Chinese University of Hong Kong in 2020. He is currently an assistant professor with The Hong Kong Polytechnic University (PolyU), Hong Kong. His research interests include the development and control of electromagnetic systems, microrobotics, and medical robotics at small scales. Dr. Yang was the recipient of the 2021 Excellent Doctoral Dissertation Nomination Award from Chinese Association of Automation (CAA), 2022 Young Scientist Finalist Award from Hong Kong Institution of Science, and Best Student Paper Award at the 2020 IEEE International Conference on Automation Science and Engineering.



**Tiantian Xu** received her M.S. in industrial engineering from Ecole Centrale Paris, France, in 2010, engineering degree in mechanics from Supmecca, France, in 2010, and Ph.D. in robotics from the Institute of Intelligent Systems and Robotics, University of Pierre and Marie Curie, Paris, France, in 2014. She was a postdoctoral fellow with the Chinese University of Hong Kong, Department of Mechanical and Automation Engineering, from 2014 to 2016. She is currently a professor with the Shenzhen Institute of Advanced Technology, Chinese Academy of Sciences. Her research interests include the design and control of magnetic robots.



**Dong Sun** received his bachelor's and master's degrees in precision instrument and mechatronics from Tsinghua University, Beijing, China, in 1990 and 1994, respectively, and a Ph.D. in robotics and automation from The Chinese University of Hong Kong, Hong Kong, in 1997. He is a chair professor at the Department of Biomedical Engineering, City University of Hong Kong. His research interests include microrobotic systems for biomedical applications and robot control. Prof. Sun is currently fellow of the Canadian Academy of Engineering, fellow of the International Academy of Medical and Biological Engineering, and fellow of the American Society of Mechanical Engineers.